ARTICLE
Journal of Cellular Biochemistry 116:2676–2694 (2015)

Journal of Cellular Biochemistry

Global Gene Deregulations in *FASN* Silenced Retinoblastoma Cancer Cells: Molecular and Clinico-Pathological Correlations

Manoharan Sangeetha,[1,2] Perinkulam Ravi Deepa,[1*] Pukhraj Rishi,[3] Vikas Khetan,[3] and Subramanian Krishnakumar[2**]

[1]*Department of Biological Sciences, Birla Institute of Technology and Science (BITS), Pilani, Rajasthan, India*

[2]*L and T Department of Ocular Pathology, Vision Research Foundation, Sankara Nethralaya, Chennai, Tamil Nadu, India*

[3]*Shri Bhagwan Mahavir Department of Vitreoretinal Services, Medical Research Foundation, Sankara Nethralaya, 18, College Road, Chennai, Tamil Nadu, India*

ABSTRACT

Activation of fatty acid synthase (FASN) enzyme in the de novo lipogenic pathway has been reported in various cancers including retinoblastoma (RB), a pediatric ocular cancer. The present study investigates lipogenesis-dependent survival of RB cancer cells and the associated molecular pathways in *FASN* silenced RB cells. The siRNA-mediated FASN gene knockdown in RB cancer cells (Y79, WERI RB1) repressed FASN mRNA and protein expressions, and decreased cancer cell viability. Global gene expression microarray analysis was performed in optimized FASN siRNA transfected and untransfected RB cells. Deregulation of various downstream cell signaling pathways such as EGFR (n = 55 genes), TGF-beta (n = 45 genes), cell cycle (n = 41 genes), MAPK (n = 39 genes), lipid metabolism (n = 23 genes), apoptosis (n = 21 genes), GPCR signaling (n = 21 genes), and oxidative phosporylation (n = 18 genes) were observed. The qRT-PCR validation in *FASN* knockdown RB cells revealed up-regulation of *ANXA1*, *DAPK2*, and down-regulation of *SKP2*, *SREBP1c*, *RXRA*, *ACACB*, *FASN*, *HMGCR*, *USP2a* genes that favored the anti-cancer effect of lipogenic inhibition in RB. The expression of these genes in primary RB tumor tissues were correlated with *FASN* expression, based on their clinico-pathological features. The differential phosphorylation status of the various PI3K/AKT pathway proteins (by western analysis) indicated that the FASN gene silencing indeed mediated apoptosis in RB cells through the PI3K/AKT pathway. Scratch assay clearly revealed that FASN silencing reduced the invading property of RB cancer cells. Dependence of RB cancer cells on lipid metabolism for survival and progression is implicated. Thus targeting FASN is a promising strategy in RB therapy. J. Cell. Biochem. 116: 2676–2694, 2015.

KEY WORDS: FATTY ACID SYNTHASE; RETINOBLASTOMA; DE NOVO LIPOGENESIS; GENE SILENCING; APOPTOSIS

Aberrant lipid metabolism is associated with various metabolic diseases, including cancer, obesity, and type-2 diabetes [Menendez et al., 2009]. Fatty acid synthase (FASN) is one of the major enzymes in de novo lipogenesis (DNL) which catalyses the conversion of acetyl and malonyl CoA into 16-carbon palmitate molecule and thus plays a crucial role in maintaining lipid

Abbreviations: RB, retinoblastoma; FASN, fatty acid synthase; siRNA, short interfering RNA; mRNA, mature RNA; qRT-PCR, quantitative real time PCR; MTT-3-(4,5-Dimethylthiazol-2-yl)-2,5, diphenyltetrazolium Bromide; ELISA, enzyme linked immunosorbant assay; PI3K, phosphoinositol 3 kinase; ANXA, annexin alpha; DAPK2, death activated kinase 2; SKP2, S-Phase kinase associated protein; CCND1, cyclin D1; SREBP1c, sterol regulatory element binding protein 1c; RXRA, retinoid x receptor alpha; USP2a, ubiquitin specific protease 2a; HMGCR, high mobility group CoA reductase; ACACB, acetyl CoA carboxylase alpha.

Grant sponsor: Indian Council of Medical Research (ICMR); Grant number: 58/9/2009-BMS.

*Correspondence to: P.R. Deepa, Department of Biological Sciences, BITS, Pilani 333031, Rajasthan, India. E-mail: dipa.bits@gmail.com

**Correspondence to: S. Krishnakumar, Vision Research Foundation, Sankara Nethralaya, 18, College Road, Chennai 600006, India. E-mail: drkrishnakumar_2000@yahoo.com

Manuscript Received: 27 January 2015; Manuscript Accepted: 5 May 2015

Accepted manuscript online in Wiley Online Library (wileyonlinelibrary.com): 8 May 2015

DOI 10.1002/jcb.25217 • © 2015 Wiley Periodicals, Inc.

homeostasis. Mammalian FASN is a multi-enzyme complex consisting of seven different domains that work together as a dimer, and is encoded by single mRNA [Stoops and Wakil, 1982]. In normal human tissues that predominantly utilize dietary fat, expression of FASN is minimal or absent, except in highly metabolic normal tissues, where the de novo fatty acid production is catalyzed by FASN, as seen in normal liver, adipocytes, cycling endometrium, and mammary cells [Menendez et al., 2009].

Lipid metabolism has become an attractive target in cancer control. Activation of de novo lipogenic pathway has been reported in various cancers (breast, ovary, prostate, melanoma, and retinoblastoma) [Pizer et al., 1996; Gansler et al., 1997; Kuhajda, 2000; Swinnen et al., 2002; Camassei et al., 2003; Vandhana et al., 2011] and is associated with tumor invasion and poor prognosis. Reduction in FASN enzyme activity by chemical inhibitors (orlistat, cerulenin, and triclosan) resulted in remarkable decrease in cancer progression in various cancer cell types [Liu et al., 2002; Zhou et al., 2003; De Schrijver et al., 2003; Menendez et al., 2004; Kridel et al., 2004; Steven et al., 2004; Browne et al., 2006; Chajes et al., 2006; Liu et al., 2008; Deepa et al., 2012]. Thus FASN has an important metabolic role in molecular pathways that regulate tumor growth and development.

Knockdown of *FASN* gene using siRNA approach has been studied in various cancer cell lines such as breast cancer cells, prostate cancer cells and ovarian cancer cells [Migita et al., 2009; Tomek et al., 2011; Gelebart et al., 2012] showing effects on energy metabolism and blockage of primary cilium formation in breast cancer and prostate cancer cells leading to apoptosis [Knowles and Smith, 2007; Willemarck et al., 2010]. Various signaling pathways such as phosphatidylinositol 3-kinase-Akt (PI3K-Akt) and LKB1/AMPK regulate the expression and activity of lipogenic enzymes via direct phosphorylation of sterol regulatory element binding proteins (SREBP) [Li et al., 2000; Yang et al., 2002]. However, signaling factors that mediate cell death while blocking FASN in cancers are largely unknown.

Retinoblastoma (RB) is the most common primary malignant intraocular tumor in children (usually below the age of 5 years). According to an estimate of 2009, around 7,202–8,102 children developed RB annually world-wide, out of which about 3,001–3,376 died of retinoblastoma annually, with most deaths reported from Asia and Africa [Kivela, 2009]. Lack of early detection, onset of metastasis at diagnosis, along with socio-economic factors and maternal health influence survival of RB patients. While in the developed countries the survival rate of RB has been nearly 90%, the survival rate in the developing countries ranges between only 40 and 79% [Canturk et al., 2010]. There is a trend away from enucleation, with the use of chemotherapy and/or combination of chemotherapy, laser, and cryotherapy, and other supportive therapies including thermotherapy, laser photocoagulation, and plaque radiation therapy showing improved benefits in some patients. However there is still a need for alternative newer treatment modalities with a better efficacy, specificity, and safety profile in RB therapy.

To our knowledge, functional knockdown of *FASN* based study of the role of lipid metabolism in RB cancer progression and control has not been reported. The present study therefore investigates the dysregulated metabolic and cell signaling pathways in *FASN*-silenced RB cells in order to understand the tumor cell survival mechanisms mediated by fatty acid synthase. Global gene expression dysregulations were examined by cDNA microarray analysis, complemented by functional validation in cultured RB cells and primary tumor tissues.

MATERIALS AND METHODS

The study was reviewed and approved by the local ethics committee of our institute, and the committee deemed that it confirmed to the generally accepted principles of research, in accordance with the Helsinki Declaration.

CELL CULTURE

Human RB cell lines, WERI-RB1 and Y79, were obtained from RIKEN BioResource Center (Ibaraki, Japan). Cells were maintained in RPMI 1640 medium (Sigma Aldrich, St. Louis, MO), supplemented with 10% fetal bovine serum (Sigma Aldrich, St. Louis, MO), 20 μg/ml streptomycin, and 20 U/ml penicillin (Invitrogen, Paisley, Germany). All cell lines were grown at 37°C in a 5% CO_2 atmosphere.

RB TUMOR SAMPLES

Informed consent was obtained from the parents of RB children for the research use of tumor samples obtained from the enucleated eyes removed as a part of treatment. The RB tumor samples were collected from 25 enucleated eyeballs of patients with RB (2011–2013). The RB sections were reviewed and graded microscopically by an ocular pathologist. The tumor samples were recorded for their clinico-pathological features (Table I) based on the predominant pattern of differentiation and tumor invasion of the choroid, optic nerve, or orbit [Sengupta et al., 2013]. The normal retina from donor cadaveric eyeballs was obtained from C U Shah eye bank, Sankara Nethralaya. [Ethical clearance no: 69-2007-P].

FASN siRNA TRANSFECTION

The WERI RB1 and Y79 cells (2×10^6) were seeded in 6-well plates (Corning, Inc., Corning, NY) with serum-free RPMI. Cells were then in vitro transfected with FASN siRNA, 5′- GAGCGUAUCUGUGA-GAAACtt-3′ and Scrambled siRNA control (All star negative control)] Qiagen (Santa Clara, CA). The FASN gene-specific siRNA was treated in the range of 50–200 nM along with lipofectamine (Invitrogen, Paisley, Germany) for 4 h at 37°C with 5% CO_2. Thereafter, 1 ml of RPMI 1640 medium containing 10% FBS were added. Cells were collected after 48 h of transfection, and used for further experiments.

GENE EXPRESSION ANALYSIS BY QRT-PCR

Real time quantitative PCR. Extraction of total RNA from FASN siRNA treated cells and primary RB tumors were performed using TRIzol reagent. For all samples 2 μg of total RNA was used to synthesize complementary DNA using Sensiscript® RT kit (QIAGEN) and random primers. Real-time PCR reactions were performed in an ABI 7300 real time PCR machine. TaqMan® Gene Expression assays for FASN (Hs00188012) and endogenous control, glyceraldehyde-3-phosphate dehydrogenase (*GAPDH*; Hs99999905_ml) [20X] Assay-

TABLE I. Clinico-Pathological Features of RB Tumor Tissues

S. No	Sample No.	Age (in years)/ sex	RB Group	Clinico-pathological characteristics	Chemotherapy details
RB tumors with invasion (n = 18)					
1	RB1	4/F	E	OD, PD, CI >3 mm. Invasion of anterior chamber trabecular meshwork, iris, ciliary body, pre-L and L invasion of ON. Tumor cells Invading anterior fibres and portion of middle fibres of sclera. The PL portion and surgical end of ON are free from tumor.	+(12 cycles)
2	RB7	9/M	E	OS, MD, Multiple focal CI by tumor cells. Invasion of IRIS stroma, tumor seen over anterior surface of iris. Invasion of pre-L, L and PL portion of ON. >3 mm	–
3	RB9	3/M	E	OS, PD, Massive CI >3 mm. pre-L, L and PL invasion of ON.	–
4	RB12	1/M	E	OD. MD, CI >3 mm, Invasion in anterior and middle portion of sclera. Invasion in Pre-L, L and PL of ON.	–
5	RB18	2/M	D	OS, PD, CI >3 mm, Tumor cells are touching the anterior fibres of the sclera, There is pre-L invasion of the ON, Surgical end of ON is free from tumor cells.	+(8 cycles)
6	RB6	6/M	E	OS, PD, Focal CI <3 mm, No invasion of Iris, invasion of cilliary process. Pre-L, L and PL invasion of ON.	–
7	RB11	4/M	E	OS. PD, Focal CI <3 mm. Pre-L & L invasion, No PL invasion	–
8	RB15	2/F	D	OD, PD, There is focal CI <3 mm. There is invasion of IRIS stroma, tumor cells seen on the iris surface, In the angle and in anterior chamber. There is pre-L invasion. There is no L and PL invasion.	+(6 cycles)
9	RB16	1/F	E	OD, MD, Focal CI <3 mm. pre-L invasion of ON. No PL and L invasion of ON. Surgical end of ON is free from tumor cells	–
10	RB17	5/F	E	OD, PD, Focal CI <3 mm, RB endophytic and exophytic combined, Invasion upto Laminar Cribrosa of ON, No invasion beyond Laminar cribrosa, Surgical end of ON is free from tumor cells.	–
11	RB24	2/M	D	OS, WD, Focal CI <3 mm. Pre-L, L invasion of ON. Separate section of surgical end is free of tumor	–
12	RB25	3/F	D	MD, CI <3 mm. Pre-L, L and minimal PL invasion of ON is seen. Surgical end of ON is free from tumor cells.	–
13	RB10	3/M	E	OD. MD, Focal retinocytoma component. No CI. Pre-L, L and PL invasion.	–
14	RB13	2/M	D	OS. MD, Minimal invasion of RPE, No CI. Pre-L invasion of ON.	–
15	RB3	1/M	E	OD, WD, Bilateral, No tumor cell in iris stroma tumor cell invading the ciliary stroma, Focal RPE invasion present. There is no invasion of Pre-L and L portion of ON. There is invasion by tumor cell in PL portion of ON. Separate sections at Surgical end of ON show tumor cell.	+(6 cycles)
16	RB2	4/F	D	OS, PD, Extensive Invasion of iris, ciliary body. Tumor seen in AC, Focal CI <3 mm. No Invasion of ON.	+(8 cycles)
17	RB8	1/F	E	OD, MD, Focal CI <3 mm, No invasion of pre-L, L &PL of ON.	–
18	RB14	2/F	E	OD. WD, Focal invasion of RPE. CI <3 mm, No invasion of ON.	–
RB tumors with no invasion (n = 7)					
19	RB4	3/F	E	OS, PD, RB endophytic and exophytic. No CI, No Invasion of ON.	–
20	RB5	2/M	E	OD, PD, endophytic and exophytic combined, No CI. No ON invasion.	+(7 cycles)
21	RB19	2/F	E	OD, Focal differentiation, No CI, pre-L, L, PL and surgical end of ON are free from tumor cells	–
22	RB20	8m/F	E	Bilateral RB, No invasion of choroid or ON.	–
23	RB21	9m/F	E	OS, MD, No invasion of ON or choroid. Surgical end is free of tumor cells.	–
24	RB22	8m/F	E	OS, WD, No invasion of ON or choroid. Surgical end is free of tumor cells	–
25	RB23	3/M	D	OS, MD, Focal retinoma component, No choroid invasion, pre-L invasion of ON. Surgical end is free of tumor cells.	–

OD, Right eye; OS, Left eye; PD, Poorly differentiated; MD, Moderately differentiated; WD, Well differentiated; ON, Optic Nerve; CI, Choroid invasion; RPE, Retinal pigment epithelium; pre-L, pre-laminar; L, laminar; PL, post laminar. The shaded rows indicate post-chemotherapy enucleation.

on-Demand gene expression assay mix was used which includes two unlabeled PCR primers (900 nM each final concentration) and FAM™ dye-labeled TaqMan® MGB (Minor Groove Binding) probe at a final concentration of 1X. Apart from primer and probe mix, a Universal Master Mix (Applied Biosystems, CA) was added. The cycling conditions were as follows: 2 min at 50°C, 10 min at 95°C and 40 cycles of 15 s at 95°C plus 1 min at 60°C, were *FASN* gene expression was normalized with *GAPDH* expression. Gene expression in each sample was analyzed in duplicate. PCR for the other genes were performed using DyNAmo Color Flash SYBR Green Master Mix in triplicates and analysed using commercial software (SDS ver. 1.3; ABI) to calculate $^{\Delta\Delta}$Ct relative expression values. Fold change for each of these genes were normalized to the *GAPDH* endogenous control (Table II). Triplicate experiments were performed and results are presented as the mean ± standard deviation.

WESTERN ANALYSIS

For western analysis, both the RB cell lines (WERI RB1, Y79) were seeded in six wells plate and transfected with FASN siRNA as mentioned above. The cells were collected in a microfuge tube and washed twice with phosphate buffered saline (PBS, 1X) solution. Centrifuged at 5,000 rpm for 5 min, and the final cell pellet was suspended in the ice cold RIPA lysis buffer (50 mmol/L Tris-Cl (pH 7.4), 1% NP40, 0.25% sodium deoxycholate, 150 mmol/L NaCl, 1 mmol/L EDTA) and 250 ml of 1 mg/ml protease inhibitor cocktail on ice. The protein concentration was estimated using Bradford reagent (Bio-rad, CA) assay at 595 nm with bovine serum albumin as standard. Protein samples (50 μg) were resolved by 8% SDS-polyacrylamide gel electrophoresis and the separated proteins were electrophoretically transferred to the nitrocellulose membrane at 100 V for 1 h. Nitrocellulose blots were treated and incubated with the following primary antibodies (BD Biosciences, NJ). Mouse monoclonal antibodies raised against human FASN (1:250), and secondary antibodies, horseradish peroxidase (HRP) conjugated goat anti-mouse IgG (1:2,000) (Santa cruz, Texas). The Phospho-AKT pathway antibody sampler kit (Cell signaling technologies, Danvers, MA) as recommended was used for checking the phosporylated status of pathway proteins. Protein loading was checked by reprobing the blot with a rabbit IgG anti-beta-actin antibody (1/1,000) (Sigma-aldrich, St. Louis). Bound antibodies were detected using the enhanced chemiluminescence Plus system (Amersham Life Sciences, Piscataway, NJ). The Biomax MR films (Eastman Kodak Company, Rochester, NY) were scanned on a Gel doc 2,000 apparatus (Biorad, Marnes-la-Coquette, France), and quantified with ImageJ analysis software. Results are presented as mean ± standard deviation of values obtained from three individual experiments.

FASN ELISA ASSAY

A total of 100 μl of total cell lysate were analyzed with a commercially available FASN ELISA kit (Cell Signaling, Danvers, MA). According to the manufacturer's recommendations, cell lysate at different concentrations of (0.1 mg, 0.2 mg, 0.3 mg, 0.4 mg and 0.5 mg/ml) were incubated in a 96-well capture plate on a plate shaker for 60 min at 37°C. The plate was then washed five times with 1X wash buffer. FASN enzyme conjugate was added and the plate was incubated for 30 min, and the wash was repeated. Total FASN levels were visualized by color change upon addition of tetramethylbenzidine substrate followed by addition of substrate stop solution. Absorbance values were read at 450 nm using a SpectraMax spectrophotometer M2 (California). FASN protein levels were compared by measuring the the absorbance values in untransfected versus transfected groups.

cDNA MICROARRAY ANALYSIS

For cDNA microarray analysis, untransfected WERI RB1 (control) and FASN siRNA transfected cells (150 nM for 48 hr) were taken. RNA extracted from both these group of cells were checked for their quality. They were then used for first- and second-strand reverse transcription, followed by a single in vitro transcription (IVT) amplification that incorporates biotin-labeled nucleotides. Sample labeling was performed using the TotalPrep RNA Amplification kit (Ambion Inc., Austin, TX) to synthesize biotin-labeled cRNA. Subsequent steps included array hybridization, washing, blocking, and streptavadin-Cy3 staining. Illumina's HumanRef-8 v2

TABLE II. List of Primer Sequences Used for qRT-PCR Analysis

Primers	Symbol		3′ to 5′
HMG CoA reductase	*HMGCR*	FP	GGACCCCTTTGCTTAGAT
		RP	CCACCAAGACCTATTGCT
S-phase kinase	*SKP2*	FP	CGTGTACAGCACATGGACCT
		RP	CCCGTTTAAGTCTCTTAGGT
Sterol regulatory element binding protein	*SREBP1c*	FP	GCCATGGATTGCACTTT
		RP	CAAGAGAGGAGCTCAATG
Retinoid X receptor	*RXRA*	FP	TCCTTCTCCCACCGCTCCAT
		RP	CAGCTCCGTCTTGTCCATCT
Acetyl CoA acyl carboxylase,Alpha	*ACACB*	FP	CAGAGCATCGTGCAGTTGGT
		RP	TGCTCAACACGCAAGTATCTTCTC
Annexin	*ANXA1*	FP	CTGCCTACCTTGCAGAGACC
		RP	TGATTGCACAGTGCCCCT
Ubiqutin specific protease-2a	*USP2a*	FP	ATGCTTGTGCCCGGTTCGAC
		RP	CTACATTCGGGAGGGCGGGCT
Cyclin D1	*CCND 1*	FP	GTGCTGCGAAGTGGAAACC
		RP	ATCCAGGTGGCGACGATCT
Fatty acid synthase	*FASN*	FP	CGACAGCACCAGCTTCGCCA
		RP	CACGCTGGCCTGCAGCTTCT
Death-associated protein kinase 2	*DAPK2*	FP	CTTTGATCTCAAGCCAGAAAAC
		RP	CTCGTAGTTCACAATTTCTGGAG

BeadChips (Illumina, San Diego,CA) were used to generate expression profiles of 47,000 probes with 500 ng of labeled cRNA for each sample as recommended by manufacturer. The BeadChips were imaged with an Illumina BeadArray Reader. The raw intensities were extracted with the Gene Expression Module in Illumina's BeadStudio software. Expression intensities were $\log_2$ transformed and median-centred by subtracting the mean value of each array from each intensity value.

CELL VIABILITY ASSESSMENT BY MTT [3-(4, 5-DIMETHYLTHIAZOL-2-YL)-2, 5 DIPHENYLTETRAZOLIUM BROMIDE] ASSAY

Cell viability in FASN siRNA transfected and untransfected RB cells was determined by MTT assay. The cells were seeded in 96-well plates at a density of 1×10^4 cells/well. After 24 h, the cells were transfected with siRNAs and cultured for 48 h. Cell proliferation was determined by adding MTT (5 mg/ml) (Invitrogen, Oregon) and incubating the cells at 37°C further for 4 h, then the precipitate was solubilized by the addition of 200 μl/well DMSO (Sigma-Aldrich, St. Louis) and shaken for 10 min. Absorbance at a wavelength of 490 nm in each well was measured with a microplate reader (Bio-Tek ELX800). Triplicate values were obtained from at least three independent experiments. Values are expressed as percentage of viable cells in transfected versus control RB cells (Test O.D./Control O.D. × 100).

ANNEXIN ASSAY

The FITC-Annexin V Apoptosis detection kit (BD, San Diego, CA) was used to detect the early and late apoptotic cells. Briefly, 2×10^6 cells (untransfected and FASN siRNA transfected) RB cells were diluted in 100 μl of Annexin V buffer, to which 5 μL of Annexin V-FITC was added subsequently. After incubation for 15 min at room temperature in the dark, 400 μl of additional binding buffer was added. Flow cytometry analysis was performed within 1 h. According to the manufacturer's protocol, Annexin V FITC-A versus Propidium Iodide-A (PI-A) with gates for following populations were prepared: a. Annexin V−/PI−; b. Annexin V+/PI−; c. Annexin V+/PI+; and d. Annexin V−/PI+. Experiments were performed in triplicate.

SCRATCH ASSAY

WERI RB1 and Y79 cells (2×10^6) were seeded in 0.01% Poly-L-lysine (Sigma Aldrich, St. Louis, MO) coated six well plates. A wound was made by scratching a straight line using a 200 ml pipette tip till confluent. The cells were then washed twice with 1× PBS, transfected with FASN siRNA as described earlier and incubated further for 48 h with 10% FBS containing media. Images were taken under 10× magnification in phase contrast microscope at 0 h, 24 h, and 48 h. The migration of cells toward the wounds was expressed as percentage of wound closure in the scratch area:

$$\% \text{ of wound closure} = [(At_0 - At_h)/At_h] \times 100\%,$$

where, At_0 is the area of wound measured immediately after scratching, and t_h is the area of wound measured 24 or 48 h after initiating the scratch.

STATISTICAL ANALYSIS

The experimental data with cultured RB cells are presented as mean ± standard deviation (SD). Student's *t*-test was used to assess statistically significant differences between groups. In RB tumor tissues analysis, groups were compared using the Mann–Whitney U-test followed by post hoc Tukey's test, and the nonparametric Spearman's rank-correlation test (Prism Graphpad statistical tool). Correlation statistics was used to relate FASN gene expression with other metabolic and cell signaling pathway gene expressions in RB tissues with varied tumor-differentiation status. All statistical tests were two-sided, and *P*-values less than 0.05 were considered as statistically significant. The 'r' values represent very weak (0.0–0.19), weak (0.2–0.39), moderate (0.4–0.59), strong (0.6–0.79), very strong (0.8–1.00) correlations.

RESULTS

EFFECTS OF FASN siRNA ON FATTY ACID SYNTHASE GENE AND PROTEIN SYNTHESIS IN HUMAN RB CANCER CELLS

Cells treated for 48 h with various concentrations of FASN siRNA (50 nM, 100 nM, 150 nM, and 200 nM) were compared with untransfected RB cells. The siRNA concentration of 150 nM resulted in FASN mRNA downregulation by −10.28 fold ($P < 0.01$) and −1.89 fold ($P < 0.01$) in WERI RB1 and Y79 respectively (Fig. 1A). These results demonstrated that the siRNA was able to effectively knockdown the expression of *FASN* in both RB cell lines. Western blot analysis showed gradual decrease in the levels of FASN protein with increasing concentrations of siRNA. Maximum down regulation was observed in the siRNA concentration of 150 nM, whereas the saturation in silencing effect was observed at 200 nM. Compared to untransfected RB cells, FASN protein expression was decreased by 86.2% in WERI RB1 and 88.5% in Y79 cells post FASN siRNA (150 nM) transfection (Fig. 1B, C). We confirmed the decrease in FASN protein levels using sandwich FASN-ELISA. Over an incremental range of total protein concentration (0.1–0.5 μg/ml) in cell-lysate, a gradual decrease of FASN in transfected cells relative to untransfected cells was observed (Fig. 1D).

CYTOTOXIC EFFECTS AND MORPHOLOGICAL VARIATION IN HUMAN RB CANCER CELLS FOLLOWING FASN siRNA TREATMENT

The silencing of FASN mRNA resulted in inhibition of cell proliferation and increased cell death in both the RB cell lines (Y79 and WERI RB1). Relative to untransfected control RB cells, viability of cells treated with 150 nM FASN siRNA (48 h) was significantly decreased to 73.33% ($P < 0.001$) and 56.36% ($P < 0.01$) in WERI RB-1 and Y79 cells respectively (Fig. 2A). The MTT assay thus revealed the gradual decrease in cell proliferation with increasing concentrations of FASN siRNA.

Based on the experimental consistency in decreasing FASN mRNA and protein levels and induction of anti-cancer cytotoxicity by 150 nM FASN siRNA, this concentration was chosen for the remaining analysis.

Abnormal cell morphology was observed post-transfection. Phase contrast microscopy revealed that the RB cancer cells started

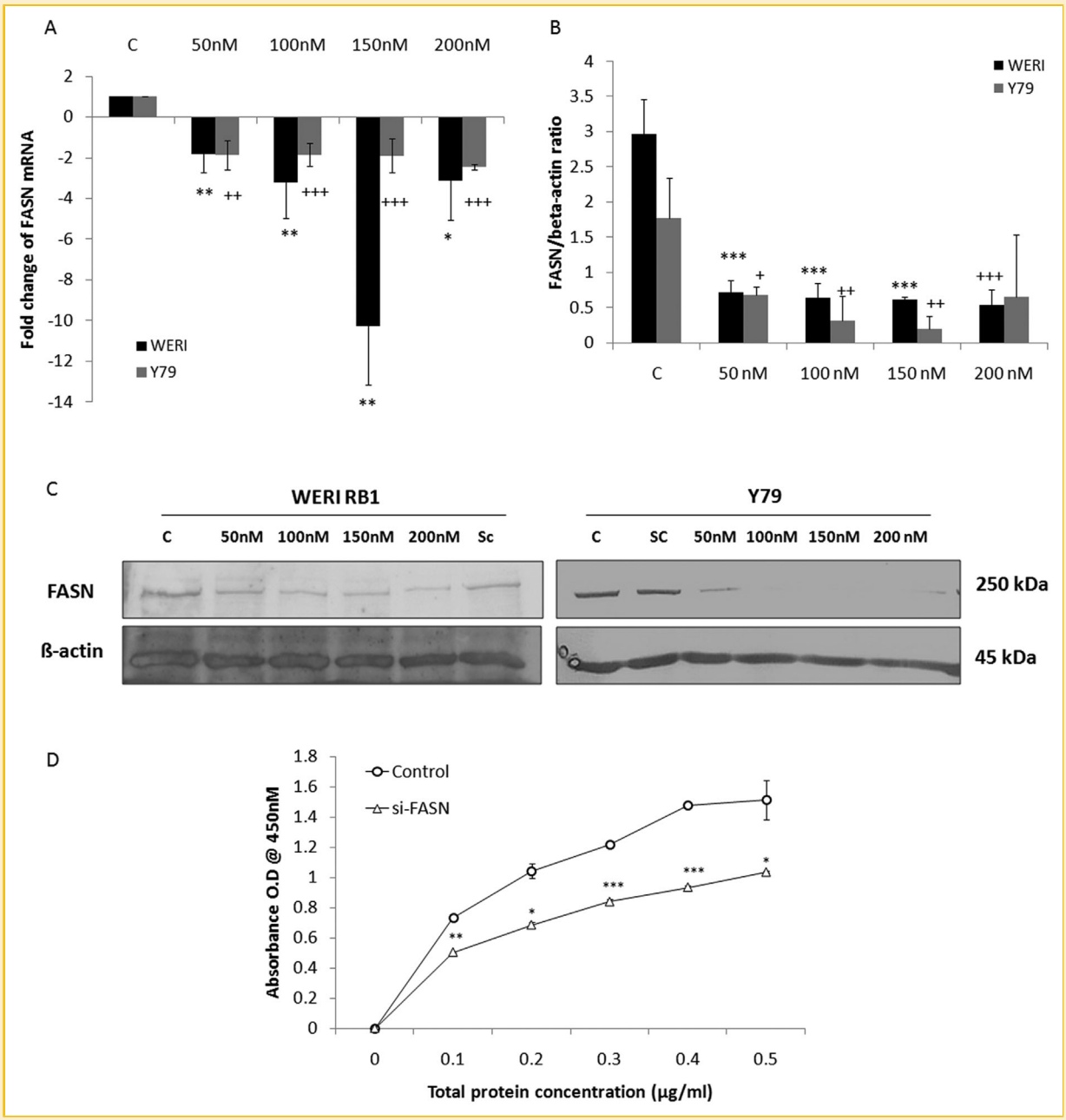

Fig. 1. Effects of FASN mRNA and protein in FASN siRNA transfected RB cells. (A) Fold change of FASN mRNA at four different concentrations of siRNA in WERI RB1 and Y79 cells compared with respective control-'C'; (B) Quantification of FASN protein levels using densitometric analysis normalized with respective ß-actin expression. C-control; (C) Representative western blot showing the effects of transfection with FASN siRNA and Sc- Scrambled siRNA on the expression of FASN in both RB cell lines; (D) Detection of FASN protein by ELISA in total protein concentration of cell lysates from FASN siRNA transfected cells compared with control WERI RB1 cell lysate. Data represents mean ± SD of three independent experiments. The symbols indicate statistical significance: $^{*}P<0.05$; $^{**}P<0.01$; $^{***}P<0.001$ compared to WERI RB1 control and $^{+}P<0.05$; $^{++}P<0.01$; $^{+++}P<0.001$ compared to Y79 control.

shrinking and assuming irregular shapes post-transfection with siRNA (Fig. 2B–E).

cDNA MICROARRAY ANALYSIS DEPICTING DIFFERENTIAL GENE EXPRESSIONS POST-TRANSFECTION

The global gene expression profile in RB cancer cells (WERI-RB1) after treatment with FASN siRNA (150 nM, 48 h) was determined by high-throughput gene expression profiling using Illumina's Human-Ref-8 v2 BeadChips. The complete dataset has been deposited in NCBI's Gene Expression Omnibus (GEO) and is accessible through GEO Series accession number (GSE63746). Proper pre-processing was applied to the values in dataset for addressing the issues of noise and missing values. Subsequently, the generated dataset was normalized with microarray data normalization methods to decrease

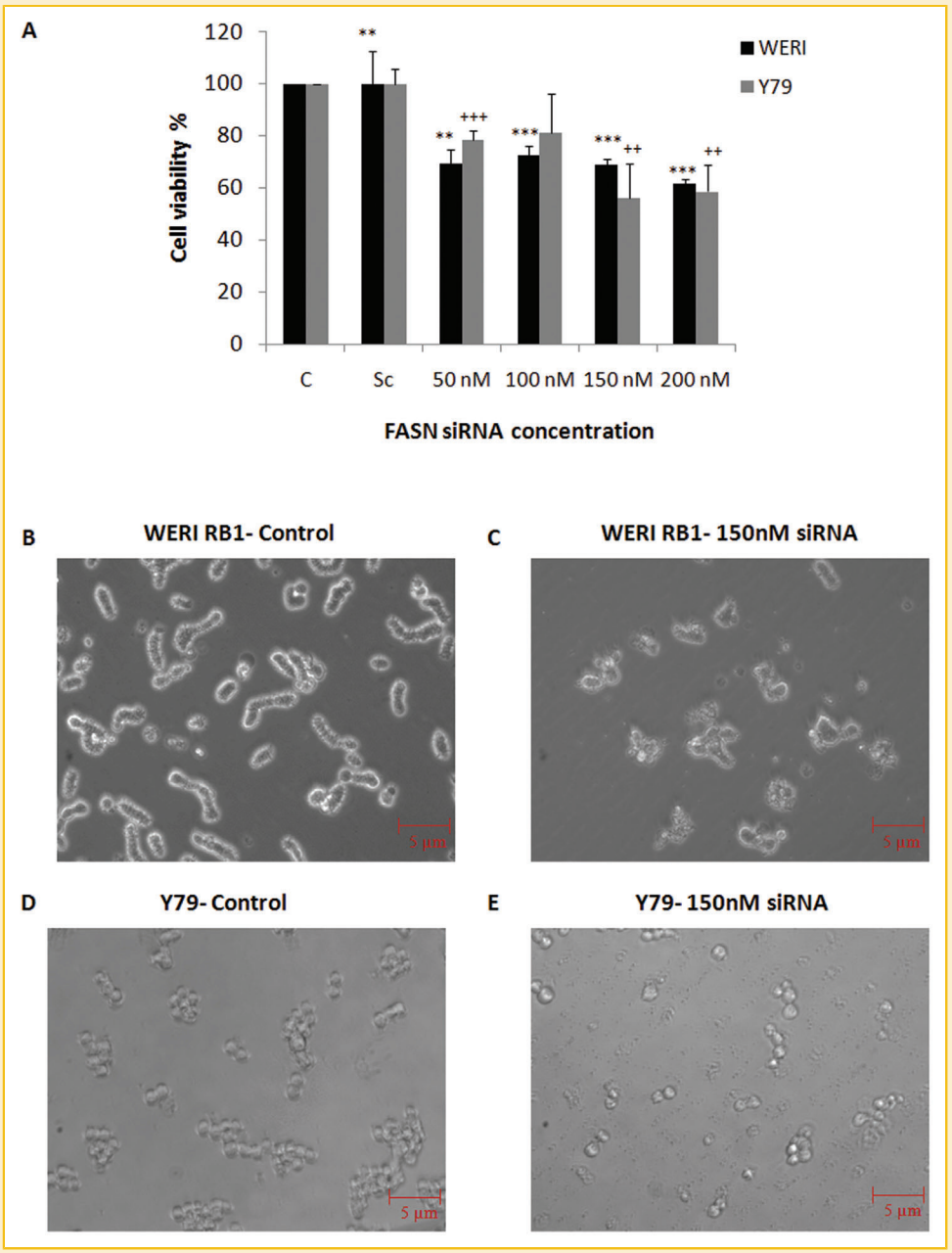

Fig. 2. Evaluation of cytotoxicity in RB cancer cells due to FASN siRNA transfection. (A) Cell viability (%) in scrambled siRNA and FASN siRNA transfected RB cell lines compared with control cells. Morphological changes due to FASN siRNA transfection observed by phase contrast microscopy in (B) WERI RB1 control; (C) WERI RB1–siRNA transfected; (D) Y79 control; (E) Y79–siRNA transfected. Data represents mean ± SD of three independent experiments. The symbols indicate statistical significance: $^{*}P < 0.05$; $^{**}P < 0.01$; $^{***}P < 0.001$ compared to WERI RB1 control and $^{+}P < 0.05$; $^{++}P < 0.01$; $^{+++}P < 0.001$ compared to Y79 control.

the number of possible false positives during the statistical selection step. Each normalized dataset was subjected to statistical testing separately and the results were combined to form the final differential expression gene lists. The fold changes between expression in untransfected control WERI RB1 cells and FASN siRNA treated WERI RB1 samples ($P < 0.05$) were listed based on fold change (≥ -1.1 to $+1.1$ in $\log_2$ scale) (Fig. 3A). This filtering yielded a list of 5,468 significantly differentiated genes. The heatmap represented the gene-expression fold where up-regulated genes are shown in red color and down-regulated genes in green.

These genes were analysed by gene ontology (KEGG database) for categorizing according to biological process and molecular function. Figure 3B shows the list of genes deregulated in major cell signaling pathways due to FASN knockdown. Interestingly, among the listed genes, large number of deregulated genes was observed in EGFR, TGF-Beta, MAPK and cell signaling pathways that are known to be involved in cell proliferation and cell invasion.

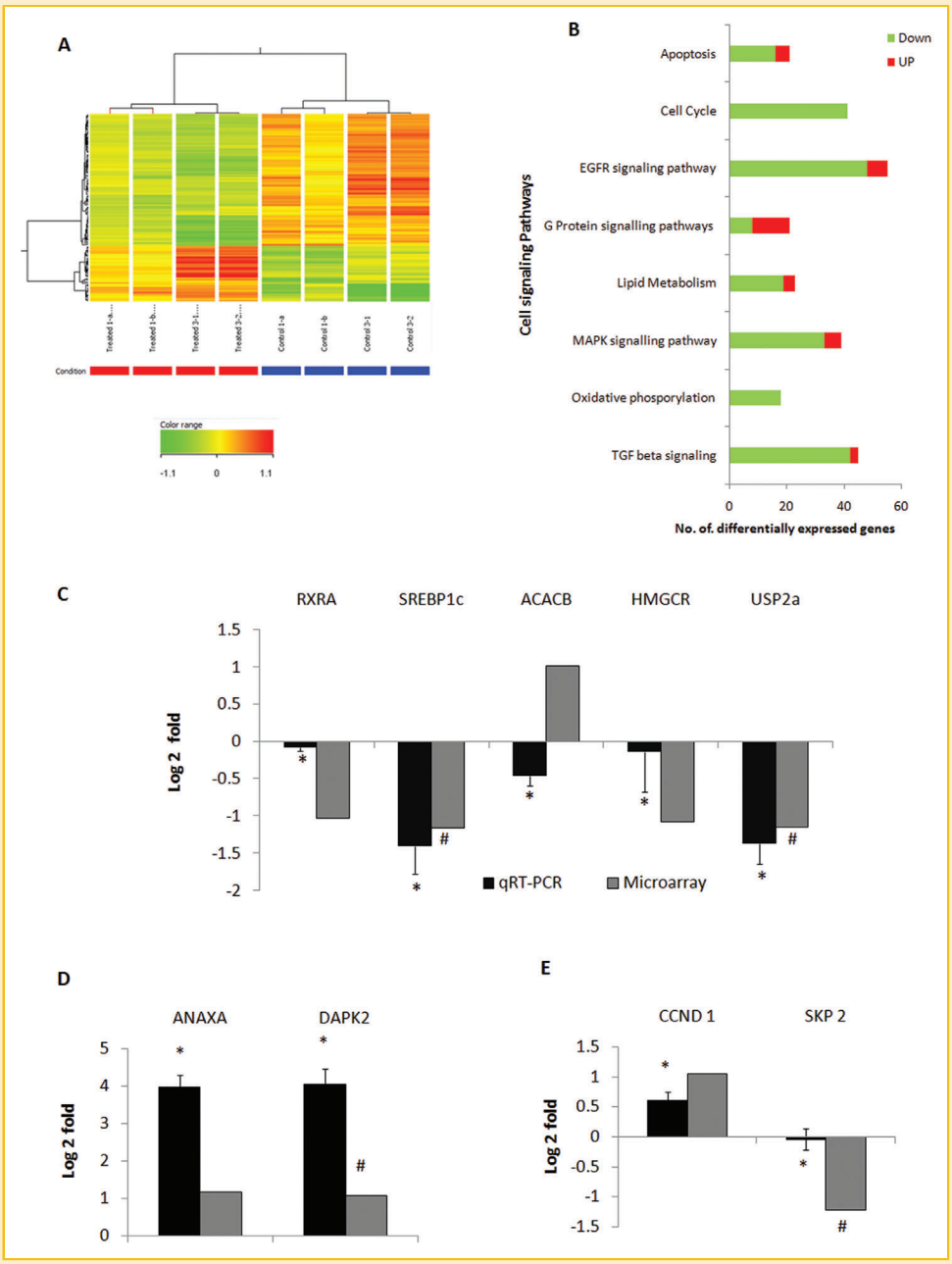

Fig. 3. cDNA microarray analysis in WERI RB1 cells transfected with FASN siRNA and validation of lipid metabolism, apoptotic and cell cycle regulator genes in FASN siRNA transfected RB cells using q-RT-PCR in comparison with microarray analysis. (A) Heatmap of differentially regulated genes ($P < 0.05$) in FASN siRNA induced gene silencing on WERI RB1 cells. Red and green indicate increased and decreased transcript expression respectively, relative to control; (B) List of overall cell signalling pathway genes deregulated due to FASN knockdown in RB. (C) Quantitative RT-PCR of FASN siRNA treated RB cells showing deregulation of genes involved in lipid metabolism (RXRA, SREBP1c, ACACB, HMGCR, Usp2a); (D) apoptosis (ANAXA, DAPK2) and (E) Cell cycle regulators (SKP2, CCND1). *Represents the statistical significance (P-value <0.05) using students t-test in qRT-PCR analysis and #represents the statistical significance (P-value <0.05) in microarray analysis using GeneSpring software.

VALIDATION OF SELECT GENES FROM MICROARRAY PROFILE BY QRT-PCR ANALYSIS

From the GO categories given in Fig. 3B, gene expression validation was performed on three categories namely lipid metabolism, cell cycle, and apoptosis, by quantitative RT-PCR analysis in RB WERI-RB1 cells (relative to untransfected cells), and also in 25 primary RB tumors (normalised to normal retina) (Table I).

The silencing of *FASN* gene showed an aberrant lipid metabolism in RB cells analysed through cDNA microarray experiments Table III. From this list, gene transcripts of *SREBP1c*, *RXRA*, *ACACB*, and *HMGCR* were validated by qRT-PCR (Fig. 3C) in RB cells treated with FASN siRNA. Consistent with the microarray results, the gene expression of the lipid metabolism related genes were down-regulated in FASN transfected RB cells except *ACACB* (+1.01 $\log_2$

TABLE III. List of Differentially Regulated Selected Genes From Microarray Analysis in WERI RB1 Cells Post siRNA Treatment

Gene Symbol	EntrezGene ID	Fold change	Regulation	*P*-value	Gene description
EGFR signaling pathway					
AKT1	207	1.08	down	0.16	v-akt murine thymoma viral oncogene homolog 1.
AP2A1	160	1.30	down	0.00	Adaptor-related protein complex 2, alpha 1 subunit.
AP2S1	1,175	1.11	down	0.00	Adaptor-related protein complex 2, sigma 1 subunit.
ARHGEF1	9,138	1.14	down	0.02	Rho guanine nucleotide exchange factor (GEF) 1.
ATF1	466	1.19	down	0.02	Activating transcription factor 1.
BCAR1	9,564	1.22	down	0.00	Breast cancer anti-estrogen resistance 1.
BRAF	673	1.14	down	0.00	v-raf murine sarcoma viral oncogene homolog B1.
EGF	1,950	1.22	up	0.03	Epidermal growth factor (beta-urogastrone).
ELK1	2,002	1.19	down	0.02	ELK1, member of ETS oncogene family.
EPS15	2,060	1.11	down	0.03	Epidermal growth factor receptor pathway substrate 15.
GRB2	2,885	1.28	down	0.01	Growth factor receptor-bound protein 2.
GSK3B	2,932	1.15	down	0.13	Glycogen synthase kinase 3 beta.
HRAS	3,265	1.18	down	0.01	v-Ha-ras Harvey rat sarcoma viral oncogene homolog.
JUN	3,725	1.35	up	0.00	Jun oncogene (JUN).
LIMK2	3,985	1.19	down	0.03	LIM domain kinase 2.
MAP2K1	5,604	1.23	down	0.02	Mitogen-activated protein kinase kinase 1.
MAP2K2	5,605	1.19	down	0.01	Mitogen-activated protein kinase kinase 2.
MAP3K3	4,215	1.16	down	0.00	Mitogen-activated protein kinase kinase kinase3.
PCNA	5,111	1.11	down	0.04	Proliferating cell nuclear antigen.
PDPK1	5,170	1.30	down	0.01	3-phosphoinositide dependent protein kinase-1 (PDPK1).
PIK3C2B	5,287	1.34	up	0.00	Phosphoinositide-3-kinase, class 2, beta polypeptide.
PIK3R1	5,295	1.16	down	0.00	Pphosphoinositide-3-kinase, regulatory subunit 1 (alpha).
PTEN	5,728	1.28	down	0.01	Phosphatase and tensin homolog.
PTK2	5,747	1.14	down	0.02	PTK2 protein tyrosine kinase 2.
PTPN12	5,782	1.16	down	0.04	Protein tyrosine phosphatase, non-receptor type 12.
RAB5A	5,868	1.23	down	0.00	RAB5A, member RAS oncogene family.
RALA	5,898	1.13	down	0.03	v-ral simian leukemia viral oncogene homolog A (ras related.
RASA1	5,921	1.28	down	0.02	RAS p21 protein activator (GTPase activating protein) 1.
SH3GL2	6,456	1.17	down	0.01	SH3-domain GRB2-like 2.
SH3GL3	6,457	1.18	down	0.02	SH3-domain GRB2-like 3.
SPRY2	10,253	1.59	up	0.05	Sprouty homolog 2.
STAM	8,027	1.56	down	0.00	Signal transducing adaptor molecule.
STAM2	10,254	1.28	down	0.00	Signal transducing adaptor molecule (SH3 domain and ITAM motif) 2.
STAT5B	6,777	1.32	down	0.03	Signal transducer and activator of transcription 5B.
USP8	9,101	1.13	down	0.05	Ubiquitin specific peptidase 8.
Cell cycle and Apoptosis					
ANXA2P2	304	1.24	up	0.00	Annexin A2 pseudogene2.
ANXA7	310	1.26	down	0.02	Annexin 7.
API5	8,539	1.15	down	0.03	Apoptosis inhibitor 5.
BNIP1	662	1.16	down	0.04	BCL2/adenovirus E1B 19kDa interacting protein 1.
BNIP2	663	1.17	down	0.03	BCL2/adenovirus E1B 19kDa interacting protein 2.
BNIP3	664	1.29	down	0.01	BCL2/adenovirus E1B 19kDa interacting protein 3 (BNIP3).
BNIP3L	665	1.13	down	0.04	BCL2/adenovirus E1B 19kDa interacting protein 3-like.
CASP3	836	1.22	down	0.01	Caspase 3, apoptosis-related cysteine peptidase.
CCNA2	890	1.24	down	0.00	Cyclin A2.
CCNC	892	1.26	down	0.00	Cyclin C.
CCND1	595	1.03	up	0.64	Cyclin D1.
CCND2	894	1.40	down	0.03	Cyclin D2.
CCNE2	9,134	1.28	down	0.01	Cyclin E2.
CCNK	8,812	1.34	down	0.03	Cyclin K (CCNK.
CCNT2	905	1.19	down	0.02	Cyclin T2.
CDK2	1,017	1.12	down	0.03	Cyclin-dependent kinase 2.
CDK2AP1	8,099	1.13	down	0.01	Cyclin-dependent kinase 2 associated protein 1.
CDK4	1,019	1.17	down	0.04	Cyclin-dependent kinase 4.
CDK5R1	8,851	1.19	down	0.00	Cyclin-dependent kinase 5.
CDK6	1,021	1.16	down	0.00	Cyclin-dependent kinase 6.
CDK7	1,022	1.17	down	0.03	Cyclin-dependent kinase 7.
CDK8	1,024	1.36	down	0.02	Cyclin-dependent kinase.
CDKL3	51,265	1.18	down	0.03	Cyclin-dependent kinase-like 3.
CDKN1C	1,028	1.15	down	0.05	Cyclin-dependent kinase inhibitor 1C.
COX10	1,352	1.15	down	0.03	COX10 homolog, cytochrome c oxidase assembly protein.
COX11	1,353	1.32	down	0.02	COX11 homolog.
COX19	90,639	1.13	up	0.03	COX19 cytochrome c oxidase assembly homolog.
COX5B	1,329	1.30	down	0.01	Cytochrome c oxidase subunit Vb.
COX7B	1,349	1.32	down	0.03	Cytochrome c oxidase subunit VIIb (COX7B).
COX7C	1,350	1.26	down	0.01	Cytochrome c oxidase subunit VIIc.
COX8A	1,351	1.18	down	0.03	Cytochrome c oxidase subunit 8A (ubiquitous).
CREBBP	1,387	1.21	down	0.00	CREB binding protein.
CREBZF	58,487	1.25	down	0.01	CREB/ATF bZIP transcription factor.
CYCSL1	157,317	1.29	down	0.04	Cytochrome c, somatic-like 1.
DAPK2	23,604	1.10	up	0.04	Death-associated protein kinase 2.
FAIM	55,179	1.19	down	0.01	Fas apoptotic inhibitory molecule.
FAIM2	23,017	1.12	up	0.03	Fas apoptotic inhibitory molecule 2.
MTBP	27,085	1.26	down	0.00	Mdm2, transformed 3T3 cell double minute 2.
MYCBP	26,292	1.18	down	0.02	c-myc binding protein.
MYCBP2	23,077	1.23	down	0.00	MYC binding protein 2.
PTGIS	5,740	1.13	up	0.03	Prostaglandin I2 (prostacyclin) synthase.

TABLE III. (*Continued*)

Gene Symbol	EntrezGene ID	Fold change	Regulation	*P*-value	Gene description
SKP2	6,502	1.25	down	0.04	S-phase kinase-associated protein 2 (p45).
TIAF1	9,220	1.20	down	0.01	TGFB1-induced anti-apoptotic factor 1.
TP53	7,157	1.44	down	0.05	Tumor protein p53.
TP53BP1	7,158	1.27	down	0.01	Tumor protein p53 binding protein 1.
TP53I13	90,313	1.12	up	0.02	Tumor protein p53 inducible protein 13.
TPRKB	51,002	1.29	down	0.00	TP53RK binding protein.
Lipid biosynthesis					
ACACB	32	1.02	up	0.74	Acetyl-Coenzyme A carboxylase beta.
ACADM	34	1.32	down	0.00	Acyl-Coenzyme A dehydrogenase, C-4 to C-12 straight chain.
ACADVL	37	1.17	down	0.04	Acyl-Coenzyme A dehydrogenase, very long chain.
ACAT2	39	1.13	down	0.04	Acetyl-Coenzyme A acetyltransferase 2.
ACBD6	84,320	1.22	down	0.01	Acyl-Coenzyme A binding domain containing 6.
ACOT9	23,597	1.17	down	0.01	Acyl-CoA thioesterase 9.
ACSBG2	81,616	1.13	up	0.04	Acyl-CoA synthetase bubblegum family member 2 .
ACSL3	2,181	1.29	down	0.01	Acyl-CoA synthetase long-chain family member 3.
DBI	1,622	1.26	down	0.01	Diazepam binding inhibitor.
ECHDC1	55,862	1.19	down	0.01	Enoyl Coenzyme A hydratase domain containing 1.
ELOVL2	54,898	1.28	down	0.01	Elongation of very long chain fatty acids.
ELOVL6	79,071	1.20	down	0.04	ELOVL family member 6.
FABP3	2,170	1.10	up	0.04	Fatty acid binding protein 3.
FADS2	9,415	1.45	down	0.04	Fatty acid desaturase 2 .
FAR1	84,188	1.17	down	0.00	Fatty acyl CoA reductase 1.
FASN	2,194	1.58	down	0.00	Fatty acid synthase.
HMGCR	3,156	1.06	down	0.36	3-hydroxy-3-methylglutaryl-Coenzyme A reductase.
IDH1	3,417	1.26	down	0.03	Isocitrate dehydrogenase 1 (NADP+), soluble.
LDLRAP1	26,119	1.23	up	0.01	Low density lipoprotein receptor adaptor protein 1.
LEPR	3,953	1.11	down	0.01	Leptin receptor.
PCCB	5,096	1.38	down	0.00	Propionyl Coenzyme A carboxylase, beta polypeptide.
PDHA1	5,160	1.16	down	0.02	Pyruvate dehydrogenase (lipoamide) alpha 1.
PDHB	5,162	1.30	down	0.00	Pyruvate dehydrogenase (lipoamide) beta.
PDHX	8,050	1.29	down	0.02	Pyruvate dehydrogenase complex, component X.
PDK3	5,165	1.32	down	0.05	Pyruvate dehydrogenase kinase, isozyme 3.
PEX13	5,194	1.40	down	0.00	Peroxisome biogenesis factor 13.
RXRA	6,256	1.03	down	0.71	Retinoid X receptor, alpha.
RXRG	6,258	1.27	down	0.00	Retinoid X receptor, gamma.
SREBF1	6,720	1.20	down	0.04	Sterol regulatory element binding transcription factor 1.
Oxidative stress					
GSTA1	2,938	1.35	up	0.02	Glutathione S-transferase alpha 1.
GSR	2,936	1.25	down	0.05	Glutathione reductase, mRNA.
GPX4	2,879	1.21	down	0.05	Glutathione peroxidase 4.
GSTA3	2,940	1.14	up	0.02	Glutathione S-transferase A3.
GSTM1	2,944	1.12	down	0.03	Glutathione S-transferase M1.
GPX7	2,882	1.11	up	0.05	Glutathione peroxidase 7.
GSTM5	2,949	1.11	up	0.02	Glutathione S-transferase M5.
SOD2	6,648	1.26	down	0.02	Superoxide dismutase 2.
NOSIP	51,070	1.25	down	0.01	Nitric oxide synthase interacting protein.
Invasion and metastasis					
ARHGEF6	9,459	1.13	up	0.05	Rac/Cdc42 guanine nucleotide exchange factor (GEF) 6.
ARHGEF9	23,229	1.28	down	0.01	Cdc42 guanine nucleotide exchange factor (GEF) 9.
ARPC3	10,094	1.29	down	0.02	Actin related protein 2/3 complex, subunit 3.
ARPC4	10,093	1.20	down	0.03	Actin related protein 2/3 complex, subunit 4
AXIN1	8,312	1.14	down	0.02	Axin 1.
AXIN2	8,313	1.19	down	0.02	Axin 2.
CDH11	1,009	1.16	down	0.05	Cadherin 11.
CDH12	1,010	1.30	down	0.02	Cadherin 12.
CTNNBL1	56,259	1.22	down	0.01	Catenin, beta like 1.
IQGAP2	10,788	1.29	down	0.02	IQ motif containing GTPase activating protein 2 (IQGAP2).
LAMB1	3,912	1.13	down	0.04	Laminin, beta 1.
LAMB4	22,798	1.19	down	0.01	Laminin, beta 4.
MMP12	4,321	1.10	up	0.04	Matrix metallopeptidase 12.
MMP15	4,324	1.15	down	0.04	Matrix metallopeptidase 15.
MTA1	9,112	1.36	down	0.00	Metastasis associated 1.
TIAM2	26,230	1.21	down	0.03	T-cell lymphoma invasion and metastasis 2

fold). The molecule responsible for the FASN protein stability, *USP2a* was found to be downregulated at its gene transcript level following FASN silencing (Fig. 3C). The apoptotic genes—*ANXA1* and *DAPK2* showed considerable up-regulation during validation. The cell cycle regulators, such as *CCND1* and *SKP2a* validated at transcript level from FASN knockdown RB cells corroborated with cDNA microarray results (*CCND1* (+1.05 $\log_2$ fold, *P*-value non-significant) and *SKP2a* (−1.22 $\log_2$ fold, *P*-value = 0.04)).

FASN-inhibition affects feedback regulation of PI3K/AKT pathway in RB. To investigate the possible molecular mechanisms underlying the cellular apoptosis of WERI RB1 after FASN silencing, changes in the expression levels of several important proteins from

the PI3K/AKT pathway (i.e., p-AKT (Thr_{308}), AKT, p-PDK1 (Ser_{241}), p-cRAF (Ser_{259}), p-PTEN (Se_{380}), and p-GSK3ß (Ser_{9})) were examined after FASN siRNA treatment (Fig. 4). The absence of phosphorylated (active) forms of AKT, PDK1, c-RAF and PTEN, concomitant with absence of phosphorylated (inactive) form of GSK3ß point to deactivation of the PI3K/AKT pathway in favor of cellular apoptosis in FASN (−) RB cells.

VALIDATION OF DEREGULATED SELECT GENES IN PRIMARY RB TUMOR TISSUES

Lipid metabolic genes including *FASN*, and select apoptotic/cell cycle regulator gene expressions were analysed using qRT-PCR in 25 RB tumor tissues (including cases of invasion, no invasion, with or without chemotherapy) (Table I). The differential gene regulations were analysed with respect to the clinico-pathological features of the tumor cohort.

Overall profile of gene deregulations in primary RB tissues. Differential mRNA expression in fold change (log_2 values) in RB tissues normalised with normal retina were represented as heatmap using conditional formatting (Fig. 5A). Fig. 5B presents the nature of deregulation of each gene in the present cohort of 25 tissue samples.

Among 10 genes analysed, Table IV presents correlations between each one of them indicating statistically significant and non-significant associations. Overall the correlation coefficient 'r' ranged between 0.768 and 0.397. Based on the 'r' values, it was observed that most genes showed moderate correlation with *FASN* (r = 0.40–0.59). *CCND1* showed weak correlation (r = 0.3621, *P*-value non-significant) and *SREBP1c*, very weak correlation (r = 0.0341, *P*-value non-significant) with *FASN* expression.

Comparison of expression of selected genes between RB tumors with and without invasion. Among the 25 tumors analysed, 17 tumors showed choroid, optic nerve and laminar (pre or post laminar) invasion while 8 tumors revealed no invasion. Within these sample groups, Mann–Whitney U-test was performed to compare the relative expressions of 10 selected genes (Table V). The median values of each gene showed clear differences in their expressions based on invasion status (although not statistically significant) (Fig. 6).

The invasive RB tumors showed an overall higher trend in gene expression compared to non-invasive RB tumors with respect to *RXRA*, *FASN*, *ACACB*, and *Usp2A* (with some very high expression values marked as outliers). The median expression of *HMGCR* appeared similar between invasion and no invasion cases, although very high expression values (outliers) were reported in invasive RB cohort. While the median tumor expression values of the pro-apoptotic genes *ANXA1* and *DAPK2* (relative to normal retina) remained less than or equal to 1, there were some upregulated values in both invasive and non-invasive tumors. It was also interesting to note that the overall expression trend of *CCND1*, *SREBP1c* and *SKP2* showed higher gene expression trend in non-invasive RB cohort than the invasive cohort, with extremely high upregulation values (outliers).

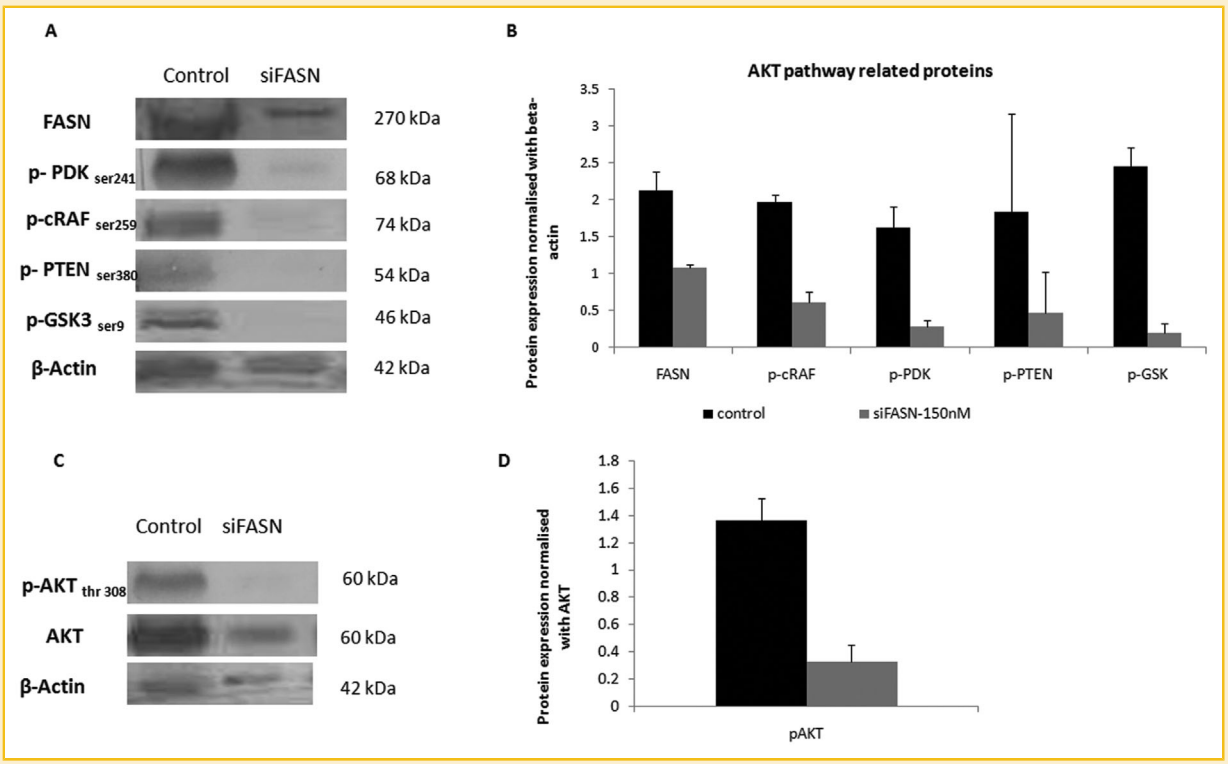

Fig. 4. Western analysis of AKT pathway proteins. (A) Representative Western blot image showing FASN protein along with AKT pathway proteins in control and FASN siRNA treated WERI RB1 cells. (B) Densitometric analysis of proteins normalised with beta-actin. (C) Representative Western blot image showing phosphorylated AKT pathway proteins in control and FASN siRNA treated WERI RB1 cells. (D) Densitometric analysis of pAKT normalised with AKT. Values are expressed as mean ± S.D. of two independent experiments.

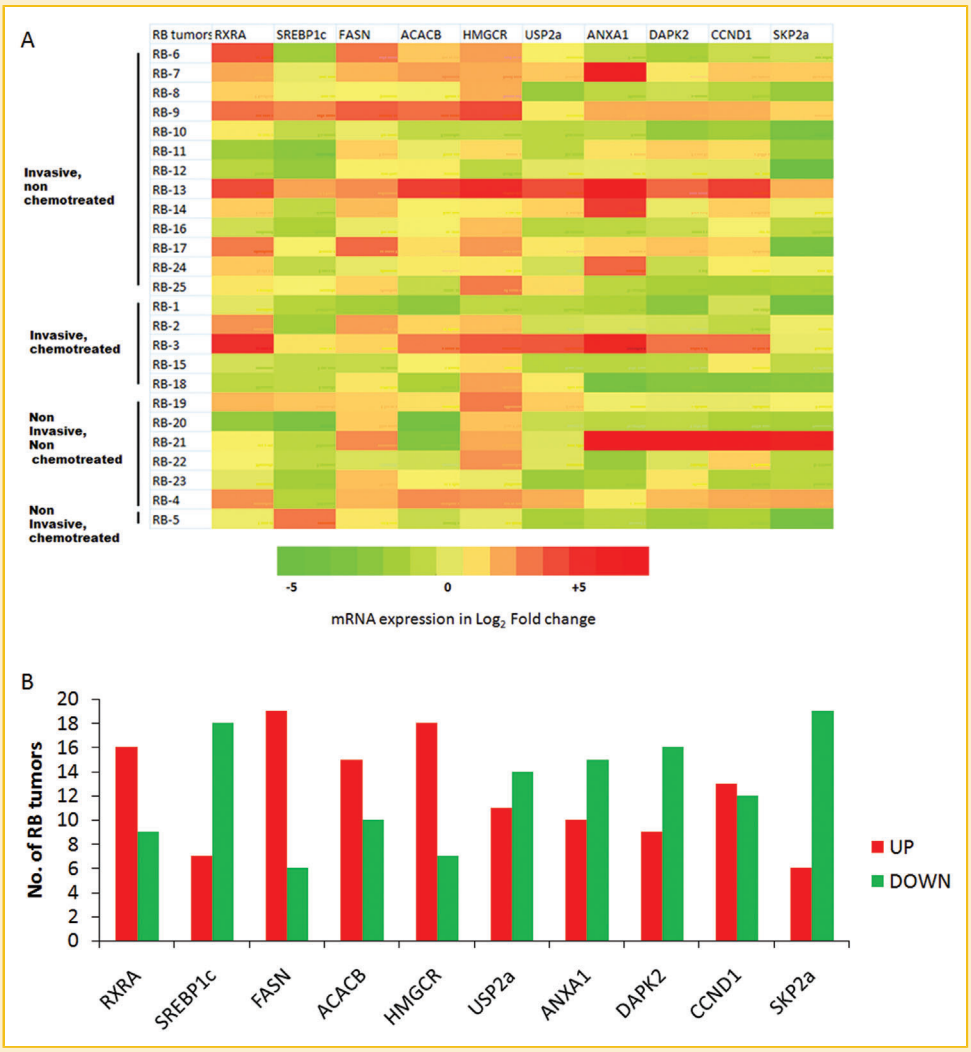

Fig. 5. (A) Heatmap showing the differential mRNA expressions of key genes involved in lipid metabolism, apoptosis and cell cycle, validated by qRT-PCR analysis of 25 primary RB tumors. (B) Number of RB tumors showing up-and down- regulations of each gene.

Correlation analysis of each gene expression relative to FASN regulation in tissues categorised by tumor differentiation status. After analysing gene expressions based on tumor invasion status we examined the clinical correlations of these genes with respect to the tumor differentiation aspect of the tumor cohort. About 28% of total RB cohort showed over-expression of *SREBP1c*. The *SREBP1c* correlated moderately ($r = 0.43$, *P*-value non significant) with the *FASN* expression in poorly differentiated RB tumors (Table VI). In contrast, the other upstream regulator of *FASN*, *RXRA* showed up-regulation in 64% ($n = 16$) in the present RB cohort (Fig. 5B). *RXRA* showed a strong correlation with *FASN* expression ($r = 0.78$, $P < 0.05$) in moderately differentiated RB tumors. The lipid synthesis pathway genes (*HMGCR* and *ACACB*) revealed strong correlation with poorly and moderately differentiated RB ($P < 0.05$).

About 60% ($n = 15/25$) and 64% ($n = 16/25$) of the overall tumor cohort showed down-regulation of pro-apoptotic genes *ANXA1* and *DAPK2* respectively (Fig. 5B). The transcriptional regulation of *ANXA1* and *DAPK2* showed very strong correlation of ($r = 0.9$ and 0.8 respectively, *P*-value non significant) with *FASN* expression in well differentiated RB tumors, and strong correlation in poorly (*ANXA1*; $r = 0.72$, $P < 0.001$) and moderately differentiated RB (*DAPK2*; $r = 0.6$, *P*-value non significant) (Table VI).

Analysis of cell cycle regulator genes showed a very strong correlation of gene expression with *FASN* in moderately and well differentiated RB tumors (*CCND1*; $r = 0.9$, *P*-value non significant, and *SKP2a*; $r = 0.85$, $P < 0.05$). The clinical and molecular interpretations have been presented in the "Discussion" section.

TARGETING FASN INDUCES CELLULAR APOPTOSIS AND SUPPRESSES CELL INVASION

Up-regulation of pro-apoptotic genes led to the activation of cellular apoptosis in *FASN* silenced RB cells (Y79 and WERI RB-1). Annexin V assay depicted the cell death induced by apoptotic mechanisms, upon *FASN* knockdown. The decrease in live cells by 52.33% was

TABLE IV. Correlation Coefficients Between the Selected 10 Genes Involved in Lipid Metabolism, Apoptosis and Cell Cycle Pathway in Primary RB Tissues

	Spearman rank correlation of the 10 genes in 25 RB tumor tissues									
	RXRA	SREBP1c	FASN	ACACB	HMGCR	USP2a	ANXA1	DAPK2	CCND1	SKP2a
RXRA										
SREBP1c	0.504**									
FASN	0.541**	0.034								
ACACB	0.748***	0.271	0.487**							
HMGCR	0.638***	0.424*	0.493**	0.472**						
USP2a	0.626***	0.338	0.474**	0.538**	0.651***					
ANXA1	0.592***	0.244	0.549**	0.537**	0.303	0.563**				
DAPK2	0.397*	0.138	0.631***	0.503**	0.448*	0.446*	0.656***			
CCND1	0.468**	0.169	0.362	0.528**	0.444*	0.509**	0.738***	0.768***		
SKP2a	0.545**	0.178	0.453**	0.518**	0.518**	0.503**	0.620***	0.545**	0.654***	

Based on the qRT-PCR analysis of fold change in gene expressions (Fig. 5), the Spearman correlation matrix for each and every gene was generated. Statistically significant values were represented as $^{*}P < 0.05$; $^{**}P < 0.01$; $^{***}P < 0.001$.

observed in the transfected WERI RB1 cells compared to untransfected control cells. Similarly, decrease in the live cells was 54% in Y79 cells transfected with FASN siRNA (Fig. 7A). These were accompanied by marked increase in apoptotic cells in the FASN silenced RB cancer cells. Taken together, the results clearly demonstrated induction of apoptotic cell death by FASN silencing.

The decreased expression of pro-invasion genes revealed by microarray analysis (Table III) prompted the wound healing assay in both the RB cell lines, with and without siRNA treatment. The percentage of wound closure at 24 h and 48 h observed in untransfected WERI RB1 cells were 56.44 and 75.91%, and in Y79 cells it was 59.30 and 65.98%, respectively. In contrast, the tumor cell invasiveness dropped to 6.92 and 5.86% in FASN siRNA transfected WERI RB1 and Y79 cells at 24 h, and by 25.56 and 38.37% in WERI RB1 and Y79 cells at 48 h, respectively. The phase contrast microscopic image (Fig. 7B and D) clearly depicts the inhibition of cell invasion in *FASN* silenced cells.

DISCUSSION

The endogenously synthesized fatty acids in cancer cells are mainly converted to phospholipids and are incorporated into the cell membranes. This fatty acid composition can have an important influence on the membrane properties, cellular functions such as cell proliferation, migration, invasion, survival and signaling at both transcriptional and post-translational levels. Earlier study characterizing two RB cell lines, Y79 and WERI RB1, revealed differential lipid composition, which reflects their differential oncogenic phenotype [Yorek et al., 1985]. The lipid composition is also strikingly different between RB cancer and normal retinal cells, as reported earlier [Vandhana et al., 2013]. All these point towards the importance of lipids and associated pathways in cell transformation.

Here we found that the *FASN* siRNA dosage of 150 nM siRNA/48 h effectively repressed *FASN* mRNA and protein levels (Fig. 1), and induced apoptotic cell death in RB cancer cells (WERI RB1 and Y79). The cell viability assay and Annexin V analysis revealed marked decrease in live cells versus increase in apoptotic cell population post-*FASN* knockdown in both the RB cells (Figs. 2 and 7A). These findings clearly indicate the definitive role of lipogenesis in RB cancer cell proliferation. Recent studies have shown that the targeted knockdown of tumor *FASN* by small molecule inhibitors or small interfering RNA (siRNA) leads to both cell cycle arrest and apoptosis in cultured cells, and suppresses tumor growth in xenograft bearing mice [Knowles et al., 2004]. This anti-tumor activity is linked to increased expression of p27kip1 [Menendez et al., 2004b] and decreased Akt phosphorylation.

TABLE V. Statistical Analysis Between Invasive and Non Invasive RB Tumor Groups: Fold Changes in Gene Expressions in the Tumor Group (Graphically Presented in Fig. 6) Are Listed Here (the 25th and 75th Percentile Values Have Been Indicated as Min. to Max. Values). Comparisons Were Done Using Mann–Whitney U-test

	Invasive			Non-invasive			
Genes	Median	Min. to	Max.	Median	Min. to	Max.	*P*-value
RXRA	2.07	0.2	48.8	1.08	0.19	5.9	0.34
SREBP1c	0.48	0.14	7.03	0.43	0.09	9.47	0.63
FASN	1.89	0.26	14.8	2.11	0.6	6.6	0.91
ACACB	1.21	0.16	31.2	0.6	0.05	6.43	0.23
HMGCR	3.16	0.42	60.3	3.76	0.8	8.6	0.83
USP2a	0.99	0.20	21.4	0.74	0.23	3.4	0.63
ANXA1	0.77	0.07	205	0.43	0.21	325	0.31
DAPK2	0.59	0.12	12.6	0.86	0.25	338	0.38
CCND1	1	0.12	30.5	0.86	0.31	263	0.97
SKP2a	0.45	0.02	3.2	0.43	0.07	106	0.43

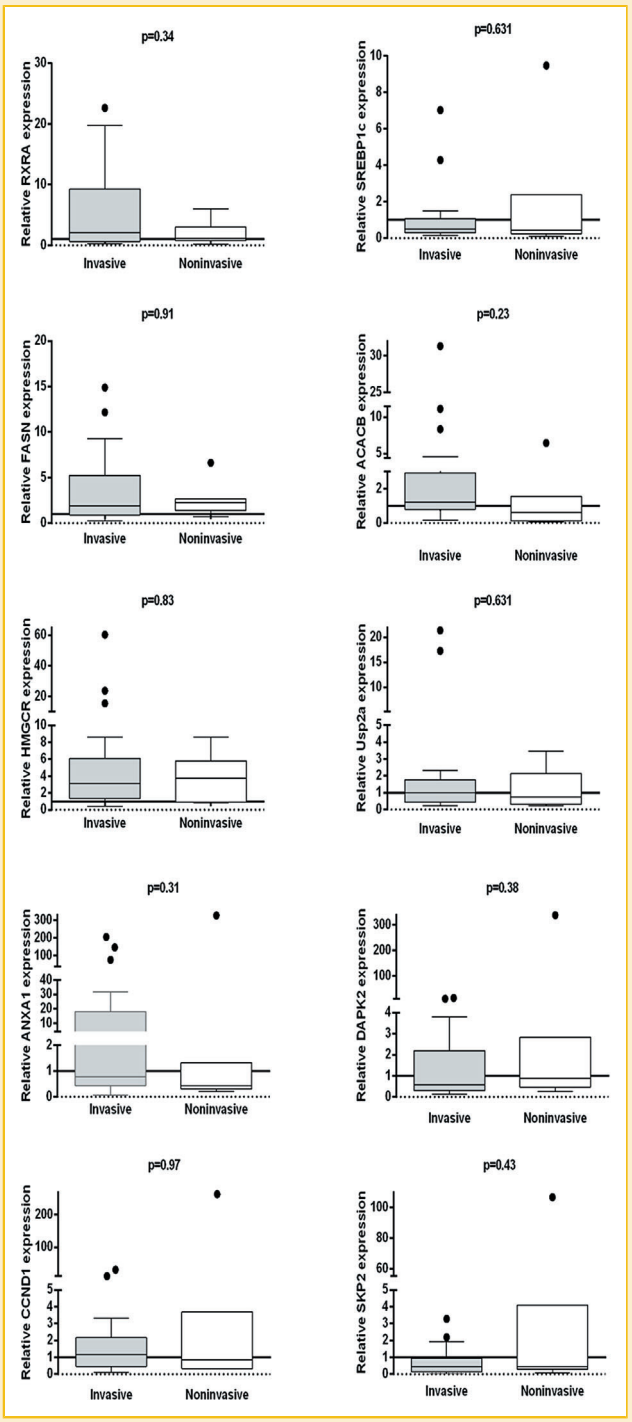

Fig. 6. Comparison of gene expressions in invasive and non invasive RB tumors. The plot shows interquartile range representing the values from the lower to upper quartile (25th to 75th percentile). The middle line within the box represents the median. The whiskers extending from the boxes represent the highest and lowest values to a multiple of 1.5 the distance of the upper and lower quartile, respectively. Post-hoc Tukey test revealed values beyond the whiskers that represent outliers (dots). Above the dotted X-axis line originating at value zero, a black line has been indicated to represent fold change = 1 (implying no differential regulation in tumor relative to normal retina).

In the present study on *FASN*-silenced RB cancer cells, the cDNA global gene microarray analysis (Fig. 3) revealed deregulation of various downstream cell signaling pathway genes including the EGFR signaling pathway, TGF-beta signaling, MAPK, cell cycle, apoptosis and lipid metabolism pathway. Validation of the genes involved in the functional pathways such as lipid metabolism, cell cycle and apoptosis, using qRT-PCR analysis correlated well with microarray data analysis (Fig. 3). There was an exception, where acetyl CoA carboxylase, a rate limiting enzyme in fatty acid synthesis, showed a statistically non-significant up-regulation (+1.01 $\log_2$ fold) in cDNA microarray analysis, but the qRT-PCR analysis showed a significant down-regulation (−0.45, log2 fold, *P*-value = 0.02). The qRT-PCR confirmation of acetyl CoA carboxylase down-regulation post *FASN* silencing was in line with the other pro-lipid synthesis gene deregulations, as *RXRA*, *SREBP1c*, *HMGCR*, and *Usp2a*. The pro-apoptotic genes such as *ANXA1* and *DAPK2* were shown to be up-regulated by both microarray and qRT-PCR analyses that suggested apoptotic cell death mechanism getting activated during lipogenic inhibition. *DAPK2* is reported to have direct link with *FASN* expression in various cancers [Bandyopadhyay et al., 2006].

One of the positive cell cycle regulators, *SKP2a* was down-regulated indicating that FASN siRNA transfection could exert its anti-cancer effect through modulation of cell division. This finding corroborates with the report by Knowles et al. [2004] in breast cancer cells. The other cell cycle regulator examined was *CCND1* which showed statistically non-significant upregulation in microarray analysis (log2 value=1.03) and in qRT-PCR analysis (log2 value = 0.606, *P*-value = 0.008). This transcriptional deregulation of *CCND1* cannot be correlated directly with FASN silencing. As discussed below in primary RB tumor validations, the correlation between *FASN* gene expressions with *CCND1* was weak.

Various signaling pathways such as phosphatidylinositol 3-kinase (PI3K)/AKT and LKB1/AMPK regulate lipogenic enzymes through direct phosphorylation of sterol regulatory element binding proteins (SREBP) [Li et al., 2000; Yang et al., 2002]. PI3K/AKT signaling plays an important role in cancer progression and has been linked with FASN expression [Wang et al., 2005]. In the present analysis, blockade of *FASN* resulted in the dephosphorylation of key proteins upstream and downstream of AKT, ultimately leading to apoptotic cell death in WERI RB1 cells (Fig. 4). In another study, *FASN* silencing altered the phosphorylation status of PI3K/AKT pathway proteins by responsive feedback loop mechanism resulting in apoptosis [Calvisi et al., 2011]. The AKT pathway proteins are differentially modulated by several factors in different cancer cell types. These include nuclear localization [Martelli et al, 2012], and different post-translational modifications such as phosphorylation, acetylation and ubiquitinylation that may affect the functional activity and stability of the pathway proteins [Khouri et al., 2005; Nakahata et al., 2014; Chan et al., 2014]. Fig. 8 illustrates the possible AKT signaling mechanism leading to cancer control in *FASN* silenced WERI RB1 cells.

In addition to evaluating the *FASN* silencing mediated cell death mechanisms and global gene deregulations in RB cancer cells in vitro, we also probed the tumor tissue expressions of these select genes (lipid metabolism, apoptosis and cell cycle regulators) in

TABLE VI. Correlation Analysis of Gene Expressions Relative to *FASN* Expression Based on Tumor Differentiation Status

	Clinico-pathological stages of RB tumor tissues					
	Poorly differentiated		Moderately differentiated		Well differentiated	
Gene	r value	*P*-value	r value	*P*-value	r value	*P*-value
RXRA	0.473	0.104	0.7857	0.048	0.100	0.95
SREBP1c	0.434	0.138	0.53	0.23	−0.7	0.233
ACACB	0.781	0.002	0.71	0.08	−0.8	0.13
HMGCR	0.643	0.02	0.57	0.2	0.1	0.95
USP2a	0.597	0.03	0.32	0.49	0.800	0.133
ANXA	0.720	0.007	0.42	0.35	0.9	0.08
DAPK2	0.586	0.03	0.6	0.16	0.800	0.133
CCND1	0.357	0.22	0.57	0.20	0.9	0.08
SKP2	0.517	0.07	0.857	0.02	0.5	0.45

Following the Spearman correlation analysis of gene expressions relative to *FASN* expression presented in Table 4, this table represents the statistical correlations based on tumor differentiation status. Bold font indicates statistically strong correlation.

primary RB cancer tissues cohort (n = 25) by qRT-PCR (Fig. 5). The cohort represented advanced stage tumors (groups D and E) with varied clinico-pathologic features and clinical interventions, where the differential gene expressions have been revealed in Fig. 5A and B. Further these gene deregulations were broadly evaluated based on (i) tumor invasion status (Fig. 6, Table V), and (ii) tumor differentiation (Table VI).

Among these genes, the pro-lipid synthesis gene regulators—*RXRA*, *FASN*, *ACACB*, and *Usp2A* had higher expressions trend in invasive cases compared to the non-invasive tumors. The median *FASN* expressions were 1.89 and 2.11 respectively in invasive and non-invasive cases. *FASN* gene showed higher expression trend in invasive RB tumors (range: 0.26–14.8) when compared with non-invasive tumors (range: 0.6–6.6). Previous report from our lab linked the *FASN* over-expression with aggressive RB tumors [Vandhana et al., 2011]. In the present cohort, the cholesterol synthesis is upregulated that is obvious from the upward trend in expression of HMG CoA reductase (HMGCR) in invasive and non-invasive tumors. One of the key upstream FASN regulators, *SREBP1c* showed a higher expression trend predominantly in the non-invasive cases (Fig. 6).

Earlier reports suggest *SREBP1c* mediated *FASN* over-expression in cancers [Huang et al., 2012; Griffiths et al., 2013] where suppressing *SREBP1c* both individually and along with FASN siRNA effectively reduced *FASN* expression leading to increased cancer cell death. In the overall cohort of RB tumor tissues, it was interesting to note that while *SREBP1c* gene expression showed a very weak correlation (r = 0.0341, *P*-value non-significant) with *FASN* expression in RB tumor tissues, there was a significant correlation between FASN expression and that of *RXRA* (r = 0.541, $P < 0.05$). While high expression of *SREBP1c* expression was reported by Li et al. [2014] in medium and poorly differentiated endometrial cancer cells, *SREBP1c* was not detected in well differentiated cells. The clinico-pathological grouping of the present RB tumors based on differentiation status (poor, moderate, and well differentiated) revealed the *SREBP1c* expression to be correlated with the poorly differentiated RB cohort (r = 0.43, *P*-value non significant).

Retinoic acid is one of the predominant lipids found in the retina of the eye required for its metabolism. The retinoic acid receptors (RAR) heterodimerize with RXR to activate lipogenesis as a cell specific co-regulatory mechanism [Lefebvre et al., 2010]. In a very recent report by Xu et al. [2014] the significance of Rb loss in RB tumors showed enhanced RXR expression involved in cone precursor tumor initiation. In our present study, the *RXRA* gene expression was predominantly up-regulated in the cohort of 25 RB tumors (up - 64%, down - 36%), and showed a significantly strong correlation with *FASN* expression (r = 0.78, $P < 0.05$) in moderately differentiated RB tumors.

The fatty acid synthesis and cholesterol synthesis pathway genes are highly expressed in most human cancers. The regulatory enzyme of fatty acid synthesis pathway ACACB, and upstream of FASN, strongly correlates with the *FASN* expression in poorly differentiated prostate tumors [Swinnen et al., 2000]. Both acetyl CoA carboxylase and FASN enzymes promote tumor cell growth, hence pharmacologic inhibitors of these enzymes are found to be useful agents in inhibiting growth of cancer cells that critically rely on fatty acid synthesis [Zhan et al., 2008].

Here, the lipid synthesising genes *ACACB* and *HMGCR* correlated significantly with *FASN* expression (*P*-value <0.05) (Table IV). The gene expressions of *ACACB* and *FASN* showed strong correlation in poorly differentiated RB (r = 0.78, $P < 0.01$) and moderately differentiated RB (r = 0.71, *P*-value non significant). In well differentiated RB, it is interesting to note that both *ACACB* and SREBP1c correlated negatively with *FASN* expression. *HMGCR* showed upregulation in 80% (n = 20/25) and down regulation in 20% (n = 5/25) of the present RB cohort. This gene correlated strongly with *FASN* expression (r = 0.64, $P < 0.05$) in poorly differentiated RB tumors. Blocking *FASN* in RB cell lines resulted in down-regulation of these lipid synthesising genes—*ACACB* and *HMGCR* (Fig. 3). Taken together, these findings clearly indicate that lipid metabolism is a strong target for RB control.

The *FASN* expression in the present tumor cohort showed differential correlations with *Usp2a*. Usp2a is a deubiqutinizing protein which maintains the stable form of FASN protein. Usp2a along with FASN and ERBB2 has been reported to have a strong correlation with well differentiated oral squamous cell carcinoma [Da Silva et al., 2009]. Table VI points to a very strong association between transcriptionally up-regulated *Usp2a* with the well-differentiated RB tumor tissues (r = 0.8, *P*-value non significant), and a significant correlation with the poorly differentiated RB with a moderate correlation (r = 0.59, $P < 0.05$). This indicates that in RB

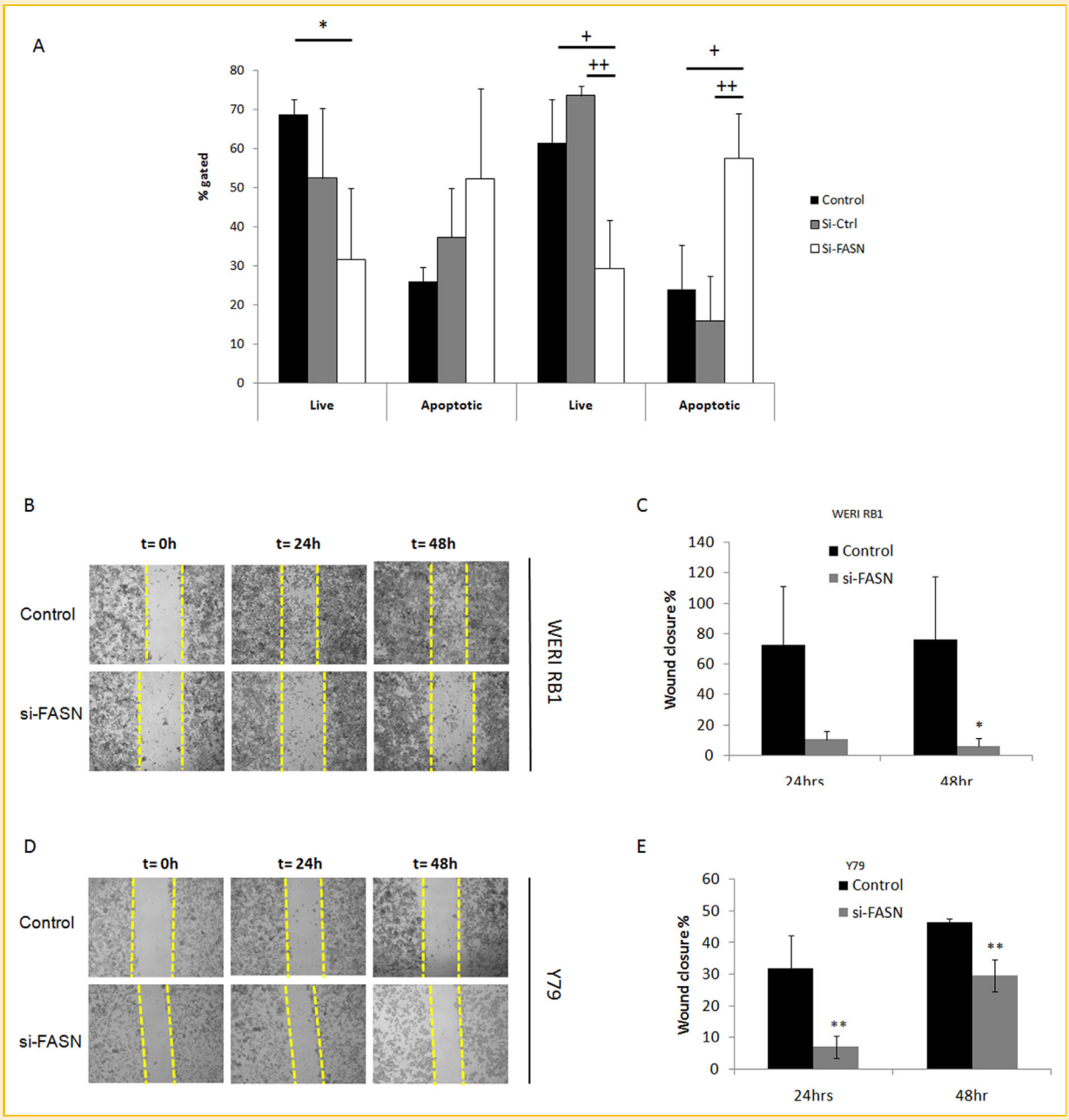

Fig. 7. (A) Annexin V assay demonstrates the increase in apoptotic cells after FASN siRNA transfection in RB cancer cells (Y79 and WERI RB 1). Data represents mean ± SD of three independent experiments. The symbols indicate statistically significant differences in values relative to Y79 control: $^{*}P < 0.05$; $^{**}P < 0.01$; $^{***}P < 0.001$; $^{+}P < 0.05$; $^{++}P < 0.01$; $^{+++}P < 0.001$ relative to WERI RB1 control. (B–E) Wound healing (scratch) assay showing significant decrease in tumor cell invasion property post transfection with FASN siRNA in WERI RB1 cells (B and C) and Y79 cells (D and E). Data represents mean ± SD of three independent experiments. Statistically significant values were represented as $^{*}P < 0.05$; $^{**}P < 0.01$; $^{***}P < 0.001$.

tumors, the post-translational stabilization of FASN protein is critical for its over-expression.

The *ANXA1* gene has a regulatory role in tumor progression and development, and can be used as a differentiation stage marker too. Its increased expression, or loss in expression, has been differentially associated with the progression of various cancer types. For instance, the loss in *ANXA1* expression has been associated with early onset of tumorigenesis in prostate cancer, head and neck carcinoma, while its increased expression is linked with advanced stage, metastasis and differentiation status in the case of breast and pituitary cancers [Lim et al., 2007]. In our study, about 60 and 64% of the overall tumor cohort showed down-regulation of pro-apoptotic genes *ANXA1* and *DAPK2* respectively. Table VI reveals the tumor differentiation stage based correlations of these pro-apoptotic gene expressions relative to *FASN* expression, where *ANXA1* and *DAPK2* showed very strong correlations in well differentiated RB. Silencing of FASN in RB

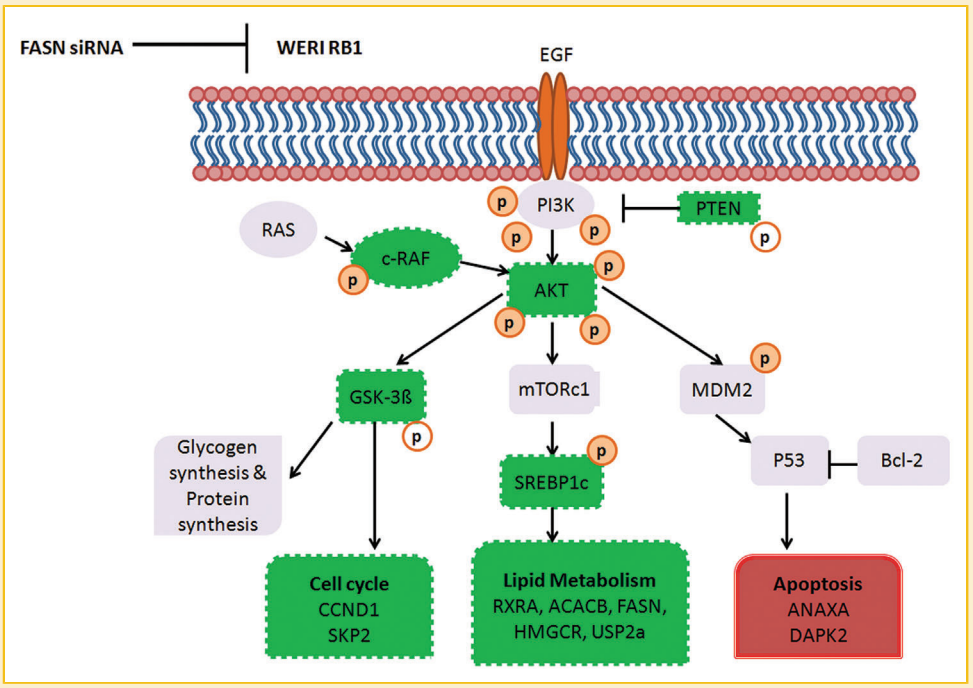

Fig. 8. Schematic illustration of PI3K/AKT cell survival pathway in RB, and their feedback control during FASN gene silencing. Based on known mechanism of AKT pathway (Yang et al., 2002) along with the present experimental findings in FASN (–) RB cells, the possible molecular regulatory network is presented. WERI RB1 cells transfected with FASN siRNA showed deregulation in AKT mediated cell survival pathway. The red and green boxes show the proteins and genes that were validated in this study. Red boxes indicate up-regulation while green boxes indicate down-regulation. Filled circles indicate active protein while phosporylated and unfilled circles represent inactive protein while phosporylated.

cancer cells resulted in marked increase in the expression of these pro-apoptotic genes (*ANXA1*: 3.9 fold, *DAPK2*: 4.0 fold).

The cell cycle regulators such as *SKP2a* and *CCND1* showed differential expressions in the present RB cohort. The overall percentage of gene up-regulations in RB tumors were 52% (*CCND1)* and 24% (*SKP2a*). Investigation based on tumor differentiation type showed a very strong correlation of *SKP2a* gene expression with *FASN* in moderately differentiated RB tumors ($r = 0.85$, $P < 0.05$). In breast cancer cells, *FASN* silencing resulted in the cell cycle arrest by down-regulation of the E3 ubiquitin ligase *SKP2a* which is involved in the stability of cellular proteins such as p27 [Knowles et al., 2004]. In the present case of RB cells too, we observed that the *FASN* gene knockdown down-regulated this pro-cell proliferation regulator, *SKP2a* (Fig. 3) that in turn led to control of RB cell growth.

The other cell cycle regulator studied was the oncogene *CCND1*. Its gene amplification, protein phosphorylation and its localization (whether in the nucleus or in the cytoplasm) are known to play functionally determining role in tumor progression [Epstein et al., 1995]. Here the *CCND1* expression in correlation with *FASN* expression was seen to be weak ($r = 0.36$) in the overall cohort of 25 RB tumor tissues. However, in well differentiated tumors the correlation with *FASN* expression was very strong ($r = 0.9$). The Cyclin D1 protein is the product *CCND1* gene and is involved in different tumor types [Peurala et al., 2013] and is correlated well with its mRNA expression. Cyclin D1 has been directly correlated with well differentiated, slow growing subtypes breast cancer tissues. While blocking *FASN* in RB cells in vitro, a mild increase in *CCND1* gene expression (log two-fold = 0.6) was observed. This finding is being interpreted with its regulator, GSK3ß′s phosphorylation status (Fig. 4). There are reports showing that the cell cycle promoting activity of CCND1 protein is suppressed by active (dephospho) form of GSK3ß, which promotes its proteosomal degradation, and thereby prevents its nuclear entry and cell cycle function [Quintayo et al., 2012]. Therefore, the GSK3ß inactivation in *FASN*-silenced RB cells here may prevent cell cycle progression involving *CCND1*.

The scratch assay analysis revealed significant reduction in invasive behavior of RB cancer cells when the FASN gene was silenced. The invasiveness of RB cancer cells (measured by wound-healing in the scratch assay) drastically reduced by 87.7 and 92.2% ($P < 0.05$) in FASN siRNA transfected WERI RB1 at 24 h and 48 h respectively. In the biologically more aggressive Y79 cells, transfected with FASN siRNA, significant reduction in invasiveness was observed (77.9% ($P < 0.01$) and 36% ($P < 0.01$) at 24 h and 48 h respectively) (Fig. 7E). This cellular effect was complemented by the molecular de-regulations observed in the microarray analysis (Table III), where FASN siRNA treated RB cells showed a significant decrease in pro-invasive genes such as metalloproteinase (*MMP15*-1.15) and laminin beta4 (*LAMB4*-1.19; *LAMB1*-1.13, *P*-value <0.05).

CONCLUSION

The relationship between lipid metabolism and cancer proliferation/control pathways in RB cancer has been analysed in this study. The

transcriptional regulation of FASN relative to key signaling genes was correlated with tumor invasion and differentiation status in primary RB tissues. FASN silencing exerted definite anti-cancer effects in RB cells through PI3K/AKT signaling pathway, and is suggested to be a promising strategy in the clinical management of RB cancer.

ACKNOWLEDGMENTS

This study was funded by Project Grant No. 58/9/2009-BMS from the Indian Council of Medical Research (ICMR), New Delhi, India. We would like to thank Mr. Madavan Vasudevan (Bionivid Technology [P] Ltd) for his help in cDNA microarray analysis and Mr. Viswanathan, Biostatistician (Vision Research Foundation, Sankara Nethralaya, Chennai) for advising us on the statistical analysis.

REFERENCES

Al-Khouri AM, Ma Y, Togo SH, Williams S, Mustelin T. 2005. Cooperative phosphorylation of the tumor suppressor phosphatase and tensin homologue (PTEN) by Casein Kinases and Glycogen Synthase Kinase 3β. J Biol Chem 280(42):35195–35202.

Bandyopadhyay S, Zhan R, Wang Y. 2006. Mechanism of apoptosis induced by the inhibition of fatty acid synthase in breast cancer cells. Cancer Res 66(11):5934–5940.

Browne CD, Hindmarsh EJ, Smith JW. 2006. Inhibition of endothelial cell proliferation and angiogenesis by orlistat, a fatty acid synthase inhibitor. Faseb J 20:2027–2035.

Calvisi DF, Wang C, Ho C, Ladu Lee, Destefanis S, Delogu G, Zimmermann S, Ericsson A, Brozzetti J, Staniscia S, Chen T, Dombrowski X, Evert F. 2011. Increased lipogenesis, induced by AKT-mTORC1-RPS6 signaling, promotes development of human hepatocellular carcinoma. Gastroenterology 140-(3):1071–1083.

Camassei FD, Cozza R, Acquaviva A, Jenkner A, Ravà L, Gareri R, Donfrancesco A, Bosman C, Vadalà P, Hadjistilianou T, Boldrini R. 2003. Expression of the lipogenic enzyme fatty acid synthase (FAS) in retinoblastoma and its correlation with tumor aggressiveness. Investig Ophthalmol Vis Sci 44:2399–2403.

Canturk S, Qaddoumi I, Khetan V, Ma Z, Furmanchuk A, Antoneli CB, Sultan I, Kebudi R, Sharma T, Rodriguez GC, Abramson DH, Chantada GL. 2010. Survival of retinoblastoma in less-developed countries impact of socioeconomic and health-related indicators. Br J Ophthalmol 94(11):1432–1436.

Chajes V, Cambot M, Moreau K, Lenoir GM, Joulin V. 2006. Acetyl-CoA carboxylase alpha is essential to breast cancer cell survival. Cancer Res 66:5287–5294.

Chan CH, Jo U, Kohrman A, Rezaeian AH, Chou PC, Logothetis C, Lin HK. 2014. Posttranslational regulation of Akt in human cancer. Cell Biosci 4:59.

Da Silva S, Cunhac IW, Nishimotob IN, Soaresc FA, Carrarod DM, Kowalskib LP, Graners E. 2009. Clinicopathological significance of ubiquitin-specific protease 2a (USP2a), fatty acid synthase (FASN), and ErbB2 expression in oral squamous cell carcinomas. Oral Oncology 45:134–139.

De Schrijver E, Brusselmans K, Heyns W, Verhoeven G, Swinnen JV. 2003. RNA interference-mediated silencing of the fatty acid synthase gene attenuates growth and induces morphological changes and apoptosis of LNCaP prostate cancer cells. Cancer Res 63:3799–3804.

Deepa PR, Vandhana S, Jayanthi U, Krishnakumar S. 2012. Therapeutic and toxicologic evaluation of anti-lipogenic agents in cancer cells compared with non-neoplastic cells. Basic Clin Pharmacol Toxicol 110(6):494–503.

Epstein JI, Carmichael M, Partin AW. 1995. OA-519 (fatty acid synthase) as an independent predictor of pathologic state in adenocarcinoma of the prostate. Urology 45:81–86.

Gansler TS, Hardman W, Hunt DA. 1997. Increased expression of fatty acid synthase (OA-519) in ovarian neoplasms predicts shorter survival. Hum Pathol 28:686–692.

Gelebart P, Zak Z, Anand M, Belch A, Lai R. 2012. Blockade of Fatty Acid Synthase Triggers Significant Apoptosis in Mantle Cell Lymphoma. PLoS ONE 7(4):e33738.DOI: 10.1371/journal.pone.0033738.

Griffiths B, Lewis CA, Bensaad K, Ros S, Zhang Q, Ferber EC, Konisti S, Peck B, Miess H, East P, Wakelam M, Harris AL, Schulze A. 2013. Sterol regulatory element binding proteindependent regulation of lipid synthesis supports cell survival and tumor growth. Cancer Metab 1:3.

Huang WC, Li X, Liu L, Lin J, Chung LWK. 2012. Activation of androgen receptor, lipogenesis and oxidative stress converged by SREBP-1 is responsible for regulating growth and progression of prostate cancer cells. Mol Cancer Res 10(1):133–142.

Kivela T 2009. The epidemiological challenge of the most frequent eye cancer: retinoblastoma, an issue of birth and death. Br J Ophthalmol 93:1129–1131.

Knowles LM, Smith JW. 2007. Genome-wide changes accompanying knockdown of fatty acid synthase in breast cancer. BMC Genomics 8:168.

Knowles LM, Axelrod F, Browne CD, Smith JW. 2004. A fatty acid synthase blockade induces tumor cell-cycle arrest by down-regulating Skp2. J Biol Chem 279(29):30540–30545.

Kridel SJ, Axelrod F, Rozenkrantz N, Smith JW. 2004. Orlistat is a novel inhibitor of fatty acid synthase with antitumor activity. Cancer Res 64(6):2070–2075.

Kuhajda FP 2000. Fatty-acid synthase and human cancer: New perspectives on its role in tumor biology. Nutrition 16(3):202–208.

Lefebvre P, Benomar Y, Staels B. 2010. Retinoid X Receptors: Common heterodimerization partners with distinct functions. Trends Endocrinol Metab 21(11):676–683.

Li JN, Mahmoud MA, Han WF, Ripple M, Pizer ES. 2000. Sterol regulatory element-binding protein-1 participates in the regulation of fatty acid synthase expression in colorectal neoplasia. Exp Cell Res 261:159–165.

Li C, Yang W, Zhang J, Zheng X, Yao Y, Tu K, Liu Q. 2014. SREBP-1 has a prognostic role and contributes to invasion and metastasis in human hepatocellular carcinoma. Int J Mol Sci 15:7124–7138.

Lim LHK, Pervaiz S. 2007. Annexin 1: The new face of an old molecule. FASEB J 21:968–975.

Liu B, Wang Y, Fillgrove KL, Anderson VE. 2002. Triclosan inhibits enoylreductase of type I fatty acid synthase in vitro and is cytotoxic to MCF-7 and SKBr-3 breast cancer cells. Cancer Chemother Pharmacol 49:187–193.

Liu H, Liu Y, Zhang JT. 2008. A new mechanism of drug resistance in breast cancer cells: Fatty acid synthase overexpression-mediated palmitate over-production. Mol Cancer Ther 7:263–270.

Martelli AM, Tabellini G, Bressanin D, Ognibene A, Goto K, Cocco L, Evangelisti C. 2012. The emerging multiple roles of nuclear AKT. Biochimt Biophys Acta 1823:2168–2178.

Menendez JA, Colomer R, Lupu R. 2004. Inhibition of tumor-associated fatty acid synthase activity enhances vinorelbine (Navelbine)-induced cytotoxicity and apoptotic cell death in human breast cancer cells. Oncol Rep 12:411–422.

Menendez JA, Mehmi I, Atlas E, Colomer R, Lupu R. 2004. Novel signaling molecules implicated in tumor-associated fatty acid synthase-dependent breast cancer cell proliferation and survival: Role of exogenous dietary fatty acids, p53-p21WAF1/CIP1, ERK1/2 MAPK, p27KIP1, BRCA1, and NF-kappaB. Int J Oncol 24(3):591–608.

Menendez JA, Martin AV, Ortega FJ, Fernandez JM. 2009. Fatty Acid Synthase: Association with Insulin Resistance, Type 2 Diabetes, and Cancer. Clin Chem 55(3):425–438.

Migita T, Ruiz S, Fornari A, Fiorentino M, Priolo F, Zadra C, Inazuka F, Grisanzio C, Palescandolo E, Shin E, Fiore C, Xie W, Kung AL, Febbo PG,

Subramanian A, Mucci L, Ma J, Signoretti S, Stampfer M, Hahn WC, Finn S, Loda M. 2009. Fatty Acid Synthase: A metabolic enzyme and candidate oncogene in prostate cancer. J Natl Cancer Inst 101:519–532.

Nakahata S, Ichikawa T, Maneesaay P, Saito Y, Nagai K, Tamura T, Manachai N, Yamakawa N, Hamasaki M, Kitabayashi I, Arai Y, Kanai Y, Taki T, Abe T, Kiyonari H, Shimoda K, Ohshima K, Horii A, Shima H, Taniwaki M, Yamaguchi R, Morishita K. 2014. Loss of NDRG2 expression activates PI3K-AKT signalling via PTEN phosphorylation in ATLL and other cancers. Nat Commun 5:3393.

Peurala E, Koivunen P, Haapasaari KM, Bloigu R, Vuorinen AJ. 2013. The prognostic significance and value of cyclin D1, CDK4 and p16 in human breast cancer. Breast Cancer Res 15:R5.

Pizer ES, Wood FD, Heine HS, Romantsev FE, Pasternack GR, Kuhajda FP. 1996. Inhibition of fatty acid synthesis delays disease progression in a xenograft model of ovarian cancer. Cancer Res 56(6):1189–1193.

Quintayo MA, Munro AF, Thomas J, Kunkler IH, Jack W, Kerr GR, Dixon JM, Chetty U, Bartlett JMS. 2012. GSK3b and cyclin D1 expression predicts outcome in early breast cancer patients. Breast Cancer Res Treat 136:161–168.

Sengupta S, Krishnakumar S, Sharma T, Gopal L, Khetan V. 2013. Histopathology of retinoblastoma: Does standardization make a difference in reporting? Pediatr Blood Cancer 60(2):336–337.

Steven JK, Fumiko A, Natasha R, Jeffrey WS. 2004. Orlistat is a novel inhibitor of fatty acid synthase with antitumor activity. Cancer Res 64:2070–2075.

Stoops JK, Wakil SJ. 1982. Animal Fatty Acid Synthetase- Identification of theresidues comprising the novel arrangement of the B-Ketoacyl synthetase site and their role in its cold inactivation. J biol chem 257(6):3230–3235.

Swinnen JV, Vanderhoydonc F, Elgamal AA, Eelen M, Vercaeren I, Joniau S, van Poppel H, Baert L, Goossens K, Heyns W, Verhoeven G. 2000. Selective activation of the fatty acid synthesis pathway in human prostate cancer. Int J Cancer 88:176–179.

Swinnen JV, Roskams T, Joniau S. 2002. Overexpression of fatty acid synthase is an early and common event in the development of prostate cancer. Int J Cancer 98:19–22.

Tomek K, Wagner R, Varga F, Singer CF, Karlic H, Grunt TW. 2011. Blockade of fatty acid synthase induces ubiqutination and degradation of phosphoinositide-3- kinase signalling proteins in ovarian cancer. Mol Cancer Res 9:1767–1779.

Vandhana S, Deepa PR, Jayanthi U, Biswas J, Krishnakumar S. 2011. Clinicopathological correlations of fatty acid synthase expression in retinoblastoma: an Indian cohort study. Exp Mol Pathol 90(1):29–37.

Vandhana. S, Coral K, Jayanthi U, Deepa PR, Krishnakumar S. 2013. Biochemical changes accompanying apoptotic cell death in retinoblastoma cancer cells treated with lipogenic enzyme inhibitors. Biochim Biophys Acta 1831:1458–1466.

Wang HQ, Altomare DA, Skele KL, Poulikakos PI, Kuhajda FP, Di Cristofano A, Testa JR. 2005. Positive feedback regulation between AKT activation and fatty acid synthase expression in ovarian carcinoma cells. Oncogene 24(22):3574–3582.

Willemarck N, Rysman E, Brusselmans K, Imschoot GV, Vanderhoydonc F, Moerloose K, Lerut E, Verhoeven G, Roy FV, Vleminckx K, Swinnen JV. 2010. Aberrant activation of Fatty acid synthesis suppresses primary cilium formation and distorts tissue development. Cancer Res 70:9453–9462.

Xu XL, Singh HP, Wang L, Qi DL, Poulos BK, Abramson DH, Jhanwar SC, Cobrinik D. 2014. Rb suppresses human cone-precursor-derived retinoblastoma tumours. Nature letters 514:385–388.

Yang T, Espenshade PJ, Wright ME, Yabe D, Gong Y, Aebersold R, Goldstein JL, Brown MS. 2002. Crucial step in cholesterol homeostasis: sterols promote binding of SCAP to INSIG-1, a membrane protein that facilitates retention of SREBPs in ER. Cell 110:489–500.

Yorek MA, Figard PH, Kaduce TL, Specror AA. 1985. A comparison of lipid metabolism in two human retinoblastoma cell lines. Invest Ophthalmol Vis Sci 26:1148–1154.

Zhan Y, Ginanni N, Tota MR, Wu M, Bays NW, Richon VM, Kohl NE, Bachman ES, Strack PR, Krauss S. Control of cell growth and survival by enzymes of the fatty acid synthesis pathway in HCT-116 colon cancer cells. Clin Cancer Res 14(8):5735.

Zhou W, Simpson PJ, McFadden JM, Townsend CA, Medghalchi SM, Vadlamudi A, Pinn ML, Ronnett GV, Kuhajda FP. 2003. Fatty acid synthase inhibition triggers apoptosis during S phase in human cancer cells. Cancer Res 63:7330–7337.